DOE/NV/13609-39

Long-term Monitoring Plan for the Shoal Underground Nuclear Test

Prepared by

Ahmed E. Hassan

submitted to

Nevada Site Office
National Nuclear Security Administration
U.S. Department of Energy
Las Vegas, Nevada

FEBRUARY 2005

Publication No. 45210

DOE/NV/13609-39

Long-term Monitoring Plan for the Shoal Underground Nuclear Test

Prepared by

Ahmed E. Hassan
Division of Hydrologic Sciences
Desert Research Institute
University and Community College System of Nevada

Publication No. 45210

Submitted to

Nevada Site Office
National Nuclear Security Administration
U.S. Department of Energy
Las Vegas, Nevada

February 2005

The work upon which this report is based was supported by the U.S. Department of Energy under Contract #DE-AC08-00NV13609. Approved for public release; further dissemination unlimited.

THIS PAGE LEFT INTENTIONALLY BLANK

EXECUTIVE SUMMARY

The groundwater flow and radionuclide transport model characterizing the Shoal underground nuclear test has been accepted by the State of Nevada Division of Environmental Protection. According to the Federal Facility Agreement and Consent Order (FFACO) between the U.S. Department of Energy and the State of Nevada, the next steps in the closure process for the site are model validation (or postaudit), proof of concept, and long-term monitoring. This report addresses the development of the monitoring strategy for Shoal, which is needed for preparing the subsurface Corrective Action Decision Document/Corrective Action Plan (CADD/CAP). The proposed monitoring plan builds on three different, yet complementary, approaches (or tools) for locating the monitoring wells around the site with the main objective being detection monitoring and the secondary objective being data collection for model validation. The purpose of a detection-based monitoring system is the identification of groundwater contamination before a plume traverses a regulatory boundary located hydraulically downgradient of the contamination source. The design of such a system entails locating monitoring wells in the areas likely to encounter plume migration.

The first tool is applied to select a number of potential siting horizons to which monitoring wells could be allocated. Based on plume geometry, this tool is used to determine the efficiency of each siting horizon and the minimum number of wells needed to span each horizon for detection monitoring. Different siting horizons can thus be ranked for detection efficiency by evaluating, for each horizon, the ratio of the maximum well spacing to the width of the potential zone of contaminant migration. A large value of this ratio indicates an effective horizon because the migration zone can be traversed with fewer wells. When a large number of monitoring wells are planned, a mathematical programming model that allocates a specified number of monitoring sites throughout the model domain can then be used. For Shoal, however, the number of monitoring wells is expected to be relatively small thereby allowing one to allocate the potential wells to the siting horizons with the highest efficiency rankings, provided that other constraints are being considered in this allocation process.

Five siting horizons or control planes (CPs) have been selected for analysis. The five CPs are oriented perpendicular to the mean flow direction, which is not parallel to the model's *y*-coordinate. The selection of the location of these CPs is aimed at providing the necessary distances from the compliance boundary for a reaction time of 50 years. The farthest CP (CP #5) passes through the western edge of the maximum contaminant level (MCL)-based contaminant boundary (assumed here to be the compliance boundary). CP #4 is located at a distance equivalent to a 50-year reaction time (about 60 m) from the farthest point on the MCL boundary. CP #3 is at a distance of 60 m from CP #5. The next CP (CP #2) passes through the eastern edge of the MCL boundary. The remaining CP (CP #1) is at a distance of 60 m from CP #2. Based on this arrangement, CP #1 is at about 360 (measured along the mean flow direction) from the working point, CP #2 is 60 m downgradient from CP #1, CP #3 is 11 m downgradient from CP #2, CP #4 is 24 m downgradient from CP #3, and CP #5 is 36 m downgradient from CP #4. By taking a 50-year reaction time from CP #2, CP #5, and the farthest northeastern point on the MCL boundary, a safeguard is provided against contaminant crossing the compliance boundary along the mean flow direction (mean plume trajectory) and from either sides of the mean trajectory.

Applying the first tool to these siting horizons indicates that the first horizon (nearest to the source) has the highest efficiency ranking (e.g., small number of wells is needed) and the efficiency decreases with increasing distance from the cavity. The minimum number of wells needed to span these horizons at different times is generally between one and two.

The second tool largely builds on the analysis conducted for the Central Nevada Test Area (CNTA) and reported in Hassan (2003). This analysis is based on using the hydrogeologic approach combined with the simulation- and probability-based approaches to place monitoring wells in locations with maximum success probability. Candidate well locations are selected along the five siting horizons with three potential well locations assigned to each horizon. The middle well at a horizon is located at the intersection of the mean flow direction and the siting horizon. The other two potential wells are selected around the central well such that they enclose 50 percent of the plume trajectories crossing each CP. In addition to these 15 well locations, another five locations were also evaluated.

The 20 total potential well locations are analyzed and their success probability is obtained. The results of this analysis show different patterns for the detection probability at different times. At 100 years, the central wells on the different CPs attain higher detection probability than the edge wells. However, for 200 and 500 years, detection probability increases from the western-edge well to the eastern-edge well. At 1,000 years, the trend is reversed and detection probability decreases from the western-edge well to the eastern-edge well. This is attributed to the interplay between the time at which detection probability is computed and the velocity encountered by each plume (thus the residence time within each well vicinity). At 100 years, only few realizations traveled far from the cavity and are located along the mean flow direction, thereby hitting the central wells. At intermediate times, fast realizations (mostly to the eastern side of the cavity and the eastern side of the mean plume trajectory) contribute to the eastern-edge wells and lead to the increase in detection probability from west to east. At late times (t = 1,000 years), the slower western realizations arrive at the different CPs and as they are migrating slowly, the particles reside for a long time within the well vicinity, thereby contributing to higher resident mass and detection probability at the western-edge wells compared to the eastern-edge wells.

Consistent with the results of applying the first tool, well 2, located at the first siting horizon, has the highest potential for success in detecting the plume. As one moves away from the cavity, success potential decreases as the variability in plume trajectory dictated by the fractured system at Shoal increases and thus the chance of a well intercepting a large number of the stochastic plumes decreases. Based on these success probabilities alone, it is difficult to maximize the benefit from the wells that will be selected. For example, if one selects the two wells with the highest success probability, they may be successful at detecting the same set of stochastic plumes, leaving a large number of equally likely plumes undetected. This, therefore, necessitates the use of another tool to evaluate the efficiency or success probability of the designed network.

The third tool is an extension to a monitoring efficiency model (MEMO) that was developed by Wilson *et al*. (1990). This model, developed for deterministic problems, is modified and extended to stochastic plumes. Seventy-six different three-well networks are selected from the 20 candidate locations and are evaluated for detection efficiency using MEMO. A rectangular detection box encompassing the three wells is used to count the number of plume trajectories that pass through and thus are likely to be detected by any of the three wells forming the evaluated network. The ratio of this number to the total number of

moving realizations (i.e., realizations whose center of mass moves beyond CP #1) is used as a measure of the network's detection efficiency. Out of the 76 networks analyzed, 28 attain detection efficiency near or above 70 percent. These results provide multiple alternatives for the locations of the three wells to be drilled for long-term monitoring at Shoal. A number of combinations are equally good and the final choice will depend on practical considerations and future agreements between model sponsor and regulators (e.g., the determination of the compliance boundary for the site).

THIS PAGE LEFT INTENTIONALLY BLANK

CONTENTS

LIST OF FIGURES

LIST OF TABLES

ACRONYMS

AMSL	above mean sea level
CADD	Corrective Action Decision Document
CAIP	Corrective Action Investigation Plan
CAP	Corrective Action Plan
c.o.m.	center of mass
CP	control plane
DDA	Data Decision Analysis
DOE	U.S. Department of Energy
DRI	Desert Research Institute
FFACO	Federal Facility Agreement and Consent Order
MCL	maximum contaminant level
NDEP	Nevada Division of Environmental Protection
NNSA	National Nuclear Security Administration
PQ	prediction quantile
PSA	Project Shoal Area
RWPT	random walk particle tracking method
UGTA	Underground Test Area

1. INTRODUCTION

The Project Shoal Area (PSA), about 50 km southeast of Fallon, Nevada, is the location of the Shoal underground nuclear test. Shoal was a 12-kiloton nuclear detonation that occurred on October 26, 1963 (U.S. DOE, 2000). The test was part of a program (Vela Uniform) to enhance seismic detection of underground nuclear tests in active earthquake areas. Figure 1 shows the location of the Shoal site relative to cities in Nevada. The PSA is the site of an ongoing environmental remediation effort that has successfully progressed through numerous technical challenges. The challenges faced are mainly caused by the substantial uncertainties present when characterizing a heterogeneous subsurface environment. Close cooperation between the U.S. Department of Energy (DOE) National Nuclear Security Administration (NNSA), the State of Nevada Division of Environmental Protection (NDEP), and supporting scientists from the Desert Research Institute (DRI) has resulted in mutual understanding and credible ways of moving forward to site closure despite knowing uncertainty will remain.

The original Corrective Action Investigation Plan (CAIP) for the PSA was approved in September 1996 and described a plan to drill and conduct testing of four characterization wells, followed by flow and transport modeling. The resultant drilling is described in a data report (DOE, 1998a) and the data analysis and modeling in an interim modeling report (Pohll *et al*., 1998). After considering the results of the modeling effort, DOE determined that the degree of uncertainty in transport predictions for Shoal remained unacceptably large. As a result, a second CAIP was developed by DOE and approved by NDEP in December 1998 (DOE, 1998b). This plan prescribed a rigorous analysis of uncertainty in the Shoal model and quantification of methods of reducing uncertainty through data collection. This analysis is termed a Data Decision Analysis (DDA) (Pohll *et al*., 1999b) and formed the basis for a second major characterization effort at Shoal. The details for this second field effort are presented in an Addendum to the CAIP, which was approved by NDEP in April 1999 (DOE, 1999). Four additional characterization wells were drilled at Shoal during summer and fall 1999; details of the drilling and well installation are in IT Corporation (2000), with testing reported in Mihevc *et al*. (2000). A key component of the second field program was a tracer test between two of the new wells (Carroll *et al*., 2000; Reimus *et al*., 2003).

The objectives of the characterization effort of this field program included the evaluation of alternative conceptual radionuclide transport models in the saturated, fractured granite and the estimation of transport parameters for use in radionuclide transport models. To achieve these objectives, a cross-hole tracer test involving the simultaneous injection of both nonsorbing and sorbing solute tracers was conducted at the site in 1999 and 2000. As a result of the tracer test and the new characterization efforts of 1999 and 2000, a new groundwater flow and radionuclide transport model was developed and approved by DOE and NDEP in 2004 (Pohlmann *et al*., 2004).

The next step in the closure process of the site is the development of the validation and long-term monitoring approaches for presentation in the Corrective Action Decision Document/Corrective Action Plan (CADD/CAP). The validation approach for the Shoal model is discussed and presented in Hassan (2004). The current report focuses on the development of the long-term monitoring network that provides site surveillance and safeguards against potential migration beyond the compliance boundary (yet to be

determined). This report largely builds on the analysis performed for the Central Nevada Test Area (CNTA) model and presented in Hassan (2003).

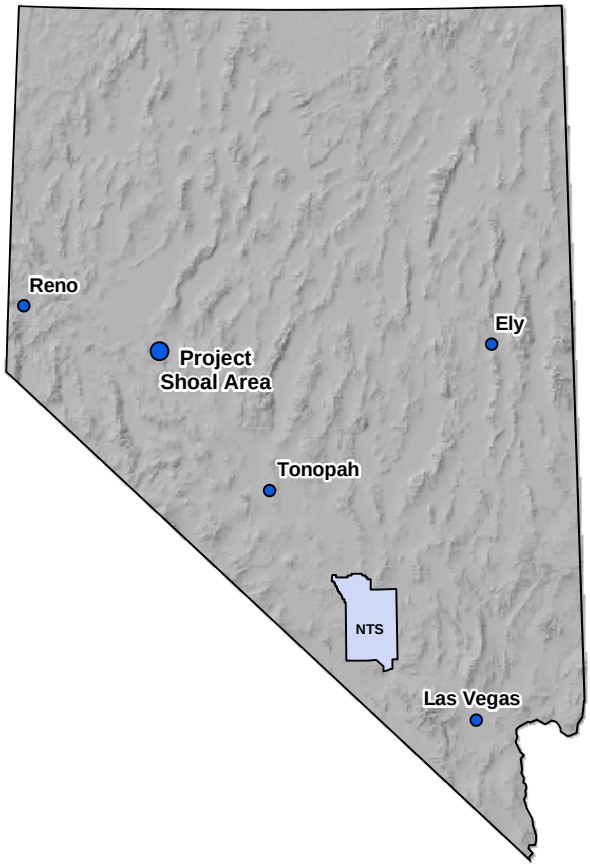

Figure 1. Location of Project Shoal Area.

Validating the stochastic Shoal model will not eliminate uncertainty from the model calculations. Confidence in the model must be explained to the public and translated into an easy-to-understand statement of acceptable risk, the risk of the incorrect decision (Chapman *et al*., 2002). Key to public acceptance is monitoring. Monitoring can be viewed as the final step addressing uncertainty in environmental problems. Groundwater monitoring not only serves to build confidence that the system is performing as predicted, it acknowledges the uncertainties inherent in the modeling process and the possibility, however remote, of unexpected outcomes. Designing a technically robust groundwater monitoring network that samples at optimum locations, times, and parameter scales is another nontrivial task (another being the validation of the stochastic Shoal model) for the PSA site.

Subsurface monitoring is generally required by regulatory agencies at groundwater sites that are already contaminated or have a potential for contamination. These include hazardous waste sites, solid waste landfills, nuclear testing sites, and other sites where the potential release or migration of contaminants is a concern. Subsurface monitoring is an expensive, time-consuming, and uncertain process. Because of these challenges, monitoring networks should be carefully designed so that the maximum amount of information is obtained with available resources. The design of a monitoring network consists of defining the number, locations, and sample pattern of sampling sites (Olea, 1984). When temporal

sampling is relevant, the sampling plan must specify the sampling frequency as well. However, prior to any sampling design, one should establish the objective of the monitoring program to deal with the question of data collection.

There is a common need to monitor the subsurface environment with a cost-effective network of wells. However, a common need does not imply common objectives. It is the set of objectives of a network that determines its specific design (Knopman *et al*., 1991). These objectives are the main factor determining the cost, the level of detail, and the appropriate method for the design of a monitoring network (Loaiciga *et al*., 1992).

As pointed out by McLaughlin and Graham (1986), there is frequently confusion over the goals of monitoring programs. Major institutional data-gathering efforts, without clearly stated goals and objectives, lead to passive groundwater quality monitoring programs that are "data-rich but information-poor" (Ward *et al*., 1986; Lee and Jones, 1983a, b). Therefore, defining quantifiable objectives is a first step in the design of cost-effective monitoring programs (Mar *et al*., 1986; Bernstein and Zalinski, 1983). It is also important that any approach to monitoring design be flexible enough to accommodate a number of different objectives that are likely to change as more data are collected.

Once the objectives of the monitoring network have been determined, the next step is to decide on the design methodology to best meet these objectives. A large body of literature exists proposing different approaches for designing groundwater monitoring networks. Different methodologies have been developed for designing monitoring networks that meet a single objective, and other methodologies have been developed for meeting multiple objectives. Hassan (2003) presents a literature review of the different design methodologies that have been developed and used for subsurface monitoring. Instead of repeating this review, the focus here is on adapting some of these approaches and applying them to Shoal for selecting the optimum locations to place monitoring wells that will be part of the long-term monitoring network at the site.

Following this introduction, Section 2 presents a brief review of the different monitoring objectives that may drive a monitoring network design and the selection of the objectives for Shoal. Section 3 then presents detailed analyses using different design tools for locating the monitoring wells that are part of the long-term monitoring network for Shoal. The report is then summarized in Section 4.

2. REVIEW OF MONITORING NETWORK OBJECTIVES

Monitoring of the subsurface environment can be performed for a number of objectives. Among these objectives are characterizing the hydrogeologic system, mapping regional variables such as the water table, and monitoring groundwater quality. A review of the different monitoring objectives and design methodologies has been presented in Hassan (2003).

In general the well network design and selection of well locations should satisfy two broad categories of objectives: 1) sampling of spatially distributed hydrogeologic variables for the purposes of aquifer characterization, and 2) sampling for subsurface pollution monitoring. However, other monitoring network objectives include such things as model discrimination (e.g., Knopman *et al*., 1991) and source identification (e.g., Mahar and Datta, 1997).

Under the general objective of subsurface characterization, monitoring network design may be performed for the purpose of characterizing the physical properties of the aquifer

(e.g., hydraulic conductivity), mapping regional variables (e.g., potentiometric map, water table elevation map, or regional groundwater flow), or for parameter estimation. Except for mapping regional variables, the other objectives under the physical characterization aspect do not receive much attention in terms of sophisticated network design efforts. More often, characterizing physical properties or estimating certain parameters is done by selecting sampling locations based on hydrogeologic expertise and general knowledge of the site under consideration.

The more common objective of monitoring networks is related to groundwater quality monitoring. Loaiciga *et al*. (1992) evaluate the various methods for network design available in the hydrologic literature by considering, among other aspects, the objective of sampling. Their review article focuses on groundwater quality monitoring networks. As mentioned earlier, other objectives can drive the monitoring network design such as parameter estimation, model discrimination, and aquifer characterization. Figure 2 shows an augmented classification of the different objectives of monitoring networks, which builds around the classification given by Loaiciga *et al*. (1992) for quality monitoring networks and extends it to include the other objectives discussed above.

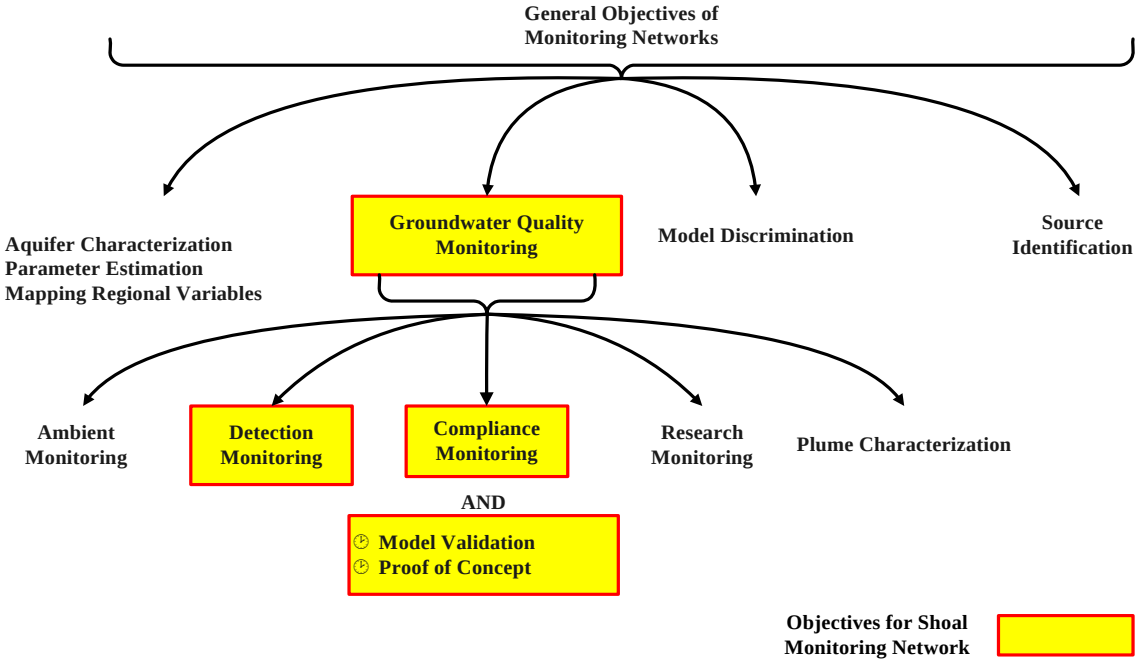

Figure 2. Classification of monitoring network objectives (or the purposes of having a monitoring well network).

As cited by Loaiciga *et al*. (1992), Todd *et al*. (1976) identified four objectives for groundwater quality monitoring activities: 1) ambient monitoring, 2) detection monitoring, 3) compliance monitoring, and 4) research monitoring. Ambient monitoring focuses on understanding the characteristics of regional groundwater quality variations over time. This type of monitoring is accomplished through routine sampling of wells on a regional basis. The wells sampled are often used for public water supply, industrial, or domestic purposes, rather than specialized monitoring wells (Loaiciga *et al*., 1992). Detection monitoring is aimed at identifying the presence of certain contaminants as soon as their concentrations exceed

background or established levels. This type of monitoring is required at and around point and nonpoint sources of groundwater contamination. The purpose of a detection-based monitoring system could also be the identification of groundwater contamination before a plume traverses a regulatory boundary located hydraulically downgradient of the contamination source (Hudak, 1994). The design of such a system entails determining the location of monitoring wells in the areas having potential for being contaminated by the plume migrating from the source.

Compliance monitoring denotes a stringent set of groundwater quality monitoring requirements for chemical compounds at a disposal facility after detecting their presence in monitoring wells. Compliance monitoring is enforced to verify the progress and success of groundwater cleanup and remediation works. Research monitoring consists of the detailed spatial and temporal groundwater quality sampling tailored to meet specific research goals (e.g., Knopman *et al*., 1991).

A monitoring network for plume characterization is designed such that an existing plume is well characterized. The objective here is to delineate the plume extent and the amount of contaminant mass within the plume area. The network design objective entails both the determination of well locations and of a sampling schedule representing sampling activities for individual wells as a function of time. The goal is to obtain monitoring networks that maximize contaminant plume characterization accuracy with a small number of active wells and a small total number of wells.

It can be seen that the long-term monitoring at Shoal should be designed to meet a number of objectives. These include compliance monitoring and detection monitoring. Under these major objectives lie other objectives such as model validation and meeting the requirements of the five-year proof of concept as per the FFACO (2000). Using the long-term monitoring data to reevaluate the model over time is considered to be a continuous model validation and postaudit process and is necessary for the long time period of concern at other nuclear testing sites. This is dictated by the fact that the behavior of hydrogeologic systems is extremely difficult to predict over extended periods of time, and uncertainties are so large that careful attention has to be paid to the possibilities of imperfect models.

As there is some similarity between detection monitoring and compliance monitoring, the remaining sections of this report focus on detection monitoring. This terminology is used in the analysis performed here to design the long-term monitoring network for Shoal. The first objective for the long-term monitoring network is to detect the presence of radionuclides in case they migrate faster than predicted. Then, the objective of assessing regulatory requirements (compliance monitoring, including model validation and proof of concept) comes into play. During the first five years of operation, the proof-of-concept monitoring is achieved where measurement of field parameters will be used to demonstrate that the model is capable of making reasonable predictions that fall within an acceptable level of confidence. This is intimately linked to the model validation and postaudit process as explained in detail in Hassan (2004).

3. MONITORING NETWORK DESIGN FOR SHOAL

Because the long-term monitoring network for Shoal will be an integral part of the CAP, all monitoring wells planned for the Shoal site must be shown (location and design) in the CAP, including existing wells that are intended to be part of the network. The CAP monitoring network must make sound scientific sense for long-term monitoring. To design a

network that makes sound scientific sense with the presence of uncertainty, a variety of tools is used for the allocation of the wells that will serve for long-term monitoring and provide data for validating the Shoal model. The use of these tools is aimed at building confidence that the selected locations are optimal locations for the objectives at hand and under the conditions of uncertainty.

As mentioned earlier, the main objective in designing the monitoring network is detection monitoring. One should select the monitoring wells in locations likely to encounter the plume migration. To design detection-based compliance monitoring in groundwater systems, either a statistical simulation or qualitative approach may be used. The former utilizes transport models to simulate the evolution of contaminants in groundwater (e.g., Massmann and Freeze, 1987a, b; Meyer and Brill, 1988; Ahlfeld and Pinder, 1988; Meyer *et al*., 1989). Each contaminant distribution is obtained from realizations of flow and transport parameters that are drawn from assumed statistical distributions. The results are used with an optimization model, which determines a monitoring well configuration from a distribution of candidate monitoring sites. The procedure is computationally intensive because groundwater flow and transport models must be utilized to generate hundreds of contaminant distributions.

A qualitative approach is based on judgments made without the use of quantitative mathematical methods (Everett, 1980; Loaiciga *et al*., 1992). Sampling locations are determined by the hydrogeologic conditions near the source of contamination. As indicated by Hudak (1994) Resource Conservation and Recovery Act (RCRA) guidelines for groundwater monitoring (EPA, 1986) specify that the placement of downgradient monitoring wells must consider: (1) the distance to the contaminant source and the direction of groundwater flow, (2) the likelihood of intercepting potential pathways of contaminant migration, and (3) the characteristics of the contaminant source controlling the movement and distribution of contamination in the aquifer. Relative to statistical simulation methods, qualitative approaches are easy to implement for field applications. However, they are highly subjective and are not well defined. Motivated by the need to overcome these limitations, Hudak (1994) developed an alternative approach for designing detection-based compliance groundwater quality monitoring networks that integrates numerical simulation of contaminant transport and mathematical programming.

3.1 First Design Tool

Hudak's (1994) approach is adapted and applied to Shoal as the first tool for selecting the number and location of detection monitoring wells. The approach is first summarized and then the flow and transport models of Shoal are used in conjunction with this approach to determine the number of wells needed at certain distances from the Shoal cavity.

3.1.1 Approach Summary

Hudak (1994) considers the hypothetical problem layout depicted in Figure 3. The objective is to detect groundwater contamination emanating from a contaminant source before it migrates to a compliance boundary. A plume can be detected by one or more monitoring wells located along various siting horizons (or control planes as employed here) oriented perpendicular to the main direction of groundwater flow. In effect, each horizon offers a potential line of defense against plume migration to the compliance boundary (Hudak, 1994). For the purpose of detection monitoring, the perpendicular orientation of siting horizons (relative to the prevailing direction of groundwater flow) is more effective than an oblique configuration. Figure 4 illustrates alternative orientations for siting horizons relative to a

common direction of groundwater flow denoted by the arrows in the figure. The tail of the arrow coincides with a hypothetical point source. In the perpendicular case, the envelope within which a plume can be detected has a wider angle at its point of origin. The perpendicular configuration thus facilitates detection of plumes emerging within a wider range of initial trajectories (Hudak, 1994).

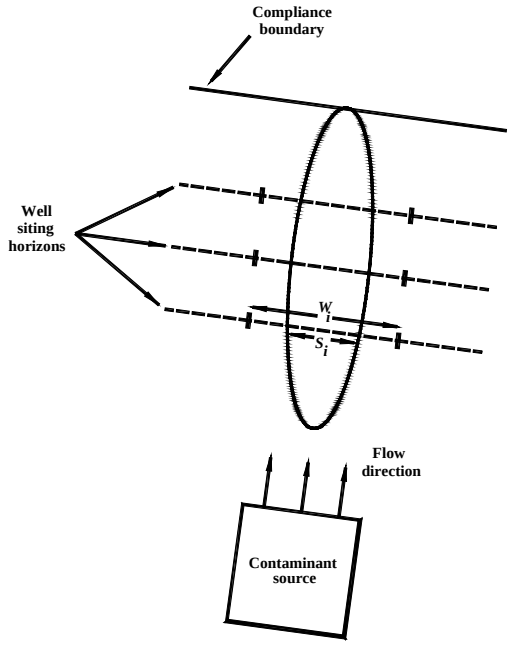

Figure 3. Schematic diagram showing the conceptualization of the source of contamination, plume migration, and siting horizons for locating monitoring wells (modified from Hudak, 1994).

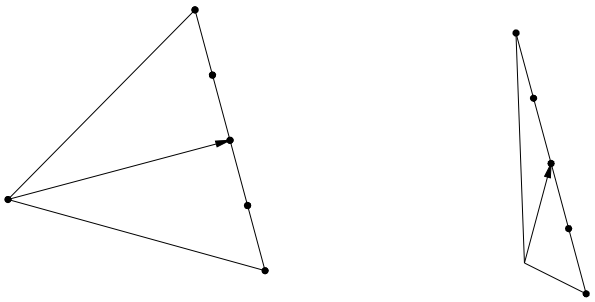

Figure 4. Detection envelopes for alternative siting horizons relative to the flow direction. Solid circles indicate potential monitoring wells (from Hudak, 1994).

In the context of detection monitoring networks for waste disposal facilities such as landfills, Hudak (1994) defines the parameters in Figure 3 as follows. A plume originating at the downgradient corner of the landfill defines a maximum well spacing, S_i, for each siting horizon, i. If a horizon is used as a line of defense against contaminant migration to the compliance boundary, the spacing between adjacent wells should not exceed S_i. Hudak's (1994) analysis considered a deterministic problem where the geometry of the zone of potential contaminant migration is defined by simulating the migration of plumes originating from various points along the perimeter of the landfill. The width of this zone, W_i, is defined

by the intersection of the siting horizon and this migration zone as shown in Figure 3. Different siting horizons can thus be ranked for detection efficiency by evaluating, for each horizon i, the ratio of the maximum well spacing, S_i, to the width of the potential zone of contaminant migration, W_i. A high S_i/W_i value indicates an effective horizon because the migration zone can be traversed with fewer wells (Hudak, 1994).

As discussed by Hudak (1994), an alternative scheme that ranks siting horizons solely on the basis of proximity to the contaminant source can lead to ineffective sampling designs. For a given application, the horizon located closest to the contaminant source is not necessarily most effective for detection monitoring. There is an inherent difficulty in detecting the contaminant plume at or near the downgradient boundary of the source because plumes tend to be relatively narrow in the initial stages of transport. Monitoring wells sited away from a source can be more effective for detecting contamination, especially if the plume has attained significant size with downgradient transport.

The approach discussed above was developed and applied to fairly simplistic and deterministic problems (e.g., Hudak, 1994, 1996, 2001). Here, it can be extended to the stochastic Shoal model with some modifications. The maximum well spacing, S_i, in the deterministic case is determined by the plume width in such a way that the plume cannot migrate between two wells without being detected. This can be replaced by the mean, mode, or any other representative statistical quantity derived from the distribution of the width of the stochastic plumes simulated at Shoal. This quantity would mean that the maximum well spacing is less than or equivalent to the plume width in a sufficiently large number of realizations. The other quantity, W_i, can be obtained for each siting horizon by, for example, computing the distance between the center of mass of the two plumes that are farthest apart. This distance represents the width of the zone of potential plume migration at the particular siting horizon.

Given values for S_i and W_i, the minimum number of monitoring wells, N_i, needed to span a horizon to ensure a well spacing that is equal to or less than S_i is given as (Hudak, 1994)

$$N_i = \lceil (W_i - 2S_i)/S_i \rceil + 1 \qquad (1)$$

where $\lceil\ \rceil$ is the ceiling function which yields the least integer that is greater than or equal to the quantity it operates on. Details of the derivation of Equation (1) can be found in Hudak (1994).

Having established a set of potential siting horizons, the corresponding ranks, and the N_i values, Hudak (1994) then presented a mathematical programming model that allocates a specified number of monitoring sites throughout the model domain. This approach, however, is necessary in cases where the number of potential monitoring wells is relatively large. Otherwise, one can easily allocate the few potential wells to the siting horizons with the highest efficiency rankings. In a typical problem, the total number of wells sited is determined by budget constraints or regulatory requirements. The detection efficiency values discussed previously can be used to reduce the number of horizons along which wells can be sited. For that purpose, S_i/W_i values would be calculated for several horizons spaced evenly between the source and compliance boundary. The analyst would then retain a subset of the horizons having the highest detection efficiency ratings. However, practical considerations and the different monitoring objectives may lead the analyst to consider siting horizons with less than optimum detection efficiency.

3.1.2 Model Domain and Transport Simulations

The Shoal model domain and some background information about the flow and transport model are presented here before the first monitoring network design tool is applied. Quantitative descriptions of numerous aspects of the conceptual flow and transport model at Shoal were needed for the numerical flow and transport models. These aspects include fracture geometry and hydraulic properties, groundwater recharge, matrix diffusion, and rates of radionuclide release from glass puddles in the cavity. All of these components contribute to the transport predictions, but the most critical are those that determine the pattern and magnitude of groundwater velocities and, as a consequence, influence the travel times of radionuclides away from the cavity. Large-scale flow and transport models have shown that the results of radionuclide transport calculations are most profoundly impacted by parameters that affect travel time (Pohll *et al*., 1999a; Pohlmann *et al*., 1999; Hassan *et al*., 2002). Naturally, all of the flow and transport parameters are subject to the uncertainties that are always present when representing subsurface conditions. These parametric uncertainties were incorporated and carried through the Shoal numerical modeling process, and were therefore ultimately included in predictions of the contaminant boundaries.

Figure 5 shows the domain for the Shoal flow and transport model, which is oriented parallel to the dominant northeast-trending structural grain of the Sand Springs Range and to the shear zone that is located near Shoal surface ground zero (SGZ) and extends northeast to

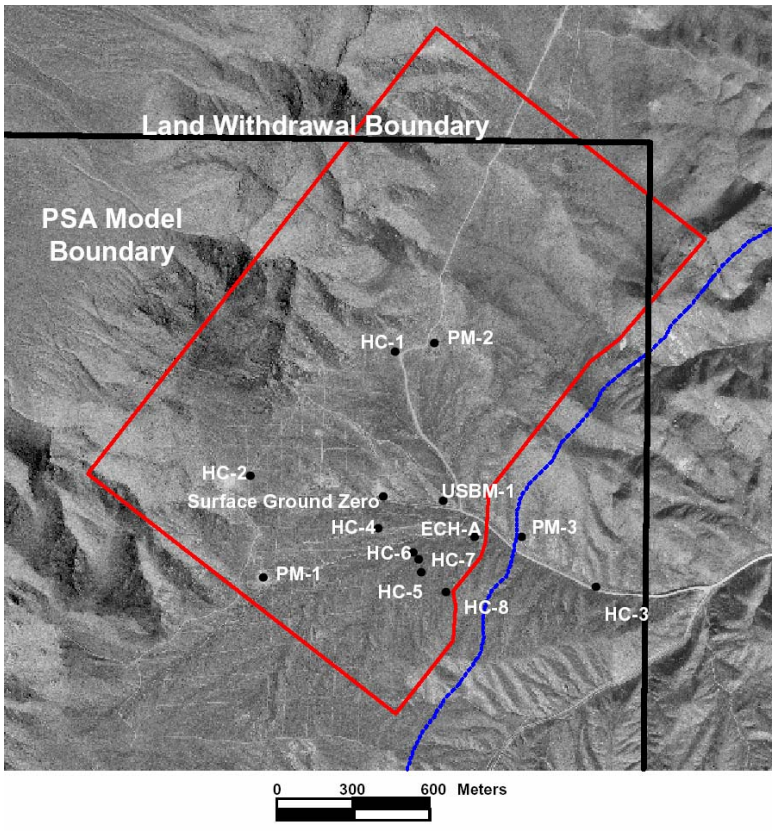

Figure 5. Map showing the domain of the Shoal flow and transport model and its location with respect to selected land surface features and the Shoal land withdrawal boundary. The blue line indicates the location of the shear zone at land surface.

the land withdrawal boundary. One thousand Monte Carlo realizations of the flow field were produced as described in Pohlmann *et al*. (2004). For the monitoring design, these flow realizations are used to perform transport simulations and obtain the geometric characteristics of the plume as it crosses a number of control planes (CPs) or siting horizons. Transport simulations are performed using the random-walk particle-tracking (RWPT) method. The RWPT code used in the Pohll *et al*. (1999) model has been substantially updated to improve the handling of the spatial variability of dispersion and porosity, improve the velocity interpolation scheme, and incorporate a new approach for simulating the matrix diffusion process. This improved code was applied to the 2004 model presented in Pohlmann *et al*. (2004). A brief overview of this approach is presented here.

Traditional random-walk methods (e.g., Kinzelbach, 1988; Tompson and Gelhar, 1990) usually rely on the assumption that medium properties such as porosity, θ, and dispersion coefficient, D, are sufficiently smooth in space. Discontinuities in effective subsurface transport properties that may arise in discrete velocity fields of numerical groundwater flow models violate this smoothness assumption (LaBolle *et al*., 2000). Therefore, when θ or D is discontinuous, these standard methods fail (LaBolle *et al*., 1996) because the gradient terms of D and/or θ cannot be formally defined. LaBolle *et al*. (2000) developed generalized stochastic differential equations applicable to the case of discontinuous coefficients (e.g., dispersion coefficients) and developed a new random-walk method that numerically integrates these equations. That method is applicable for cases of abrupt changes in transport parameters and velocity values. The new random-walk equations proposed by LaBolle *et al*. (2000) can be written as

$$\boldsymbol{X}_{t+\Delta t} = \boldsymbol{X}_t + \left[\boldsymbol{V}(\boldsymbol{X}_t, t)\right]\Delta t + \left[2\mathbf{D}(\boldsymbol{V}(\boldsymbol{X}_t + \delta\boldsymbol{X}), t)\Delta t\right]^{1/2} \cdot \boldsymbol{Z} \qquad (2)$$

where the displacement vector $\delta\boldsymbol{X}$ is defined as

$$\delta\boldsymbol{X} = \left[2\mathbf{D}(\boldsymbol{V}(\boldsymbol{X}_t, t))\Delta t\right]^{1/2} \cdot \boldsymbol{Z} \qquad (3)$$

The approach evaluates the advective component of particle movement using the velocity at the current particle position, (x_t, y_t, z_t), and at time t. The dispersive component is performed using dispersion coefficients evaluated at an intermediate location, $(x_t + \delta x, y_t + \delta y, z_t + \delta z)$, where the increments δx, δy, and δz represent dispersive steps from the current location, (x_t, y_t, z_t) to the intermediate location $(x_t + \delta x, y_t + \delta y, z_t + \delta z)$. The details of the approach and how it is incorporated in the RWPT code are described in Pohll *et al*. (2002).

The transport approach described thus far is appropriate for a porous medium; however, the conceptualization of the flow system at Shoal includes fractured granite, which has correspondingly high flow velocities adjacent to unfractured porous zones. A continuum approach is applied in the sense that effective fracture properties (high K and low porosity) are assigned to the model cells rather than direct incorporation of discrete fractures. As a result, particles are tracked through space in the same manner as for a porous medium, but they experience high flow velocities when they pass through a fracture cell.

Although the RWPT code accounts for matrix diffusion and the interaction between fluids in the fractures and fluids in the matrix, for the monitoring design analysis here, this process is not included in the analysis. This is simply because the interest here is in the geometric characteristics of the plume without regard to the values of the mass flux

breakthrough curves or the values of contaminant concentrations. The results presented here could essentially be obtained with matrix diffusion included but with a much larger number of particles than used here, which would unnecessarily increase computation time. Also, the focus here is only on the nonsorbing transport (Class #1's radionuclides) and as such, no retardation is considered. This is again due to the focus on the physical and geometric aspects of the plume as it crosses the selected CPs.

The transport calculations are conducted using the same grid discretization and domain size as the groundwater flow model (Pohlmann *et al*., 2004). The radionuclide source is assumed to be the entire Shoal cavity, which is simulated in the model as a sphere having a diameter of 40 m (the estimated cavity radius is 26 m [Hazelton-Nuclear Science, 1965], but is approximated in the model by the constraints of the grid size of 20 m^3 blocks). The values of the transport parameters that are not treated as uncertain as well as the range of parameters treated as uncertain are listed in Table 1. The time step length for each realization is calculated within the RWPT code using the values of porosity for the different categories associated with that realization. Time step lengths are chosen so that the Courant numbers for any realization are less than one to ensure that particles are not transported a distance equal to the dimension of one grid cell (20 m) in a single time step.

Table 1. Values of parameters that describe the configuration of the transport model and values of deterministic parameters. Ranges of uncertain parameters are also presented.

Parameter	Value
Location of Source, World Coordinates	
Easting (m)	380808
Northing (m)	4339630
Elevation (m AMSL)	1,220
Location of Source, Model Coordinates	
x (m)	1,211
y (m)	540
z (m)	1,220
Radius of Cavity (m)	20
Total Simulation Time (years)	1,000
Longitudinal Dispersivity (m)	2.0
Transverse Dispersivity (m)	0.2
Retardation (dimensionless)	
Damaged Zone	1.0
Cavity	1.0
Porosity (dimensionless)	
Matrix	0.015
Fractures	0.005 to 0.07
Damaged Zone	0.07 to 0.18
Cavity	0.18 to 0.35
Fracture Spacing (m)	0.5
Number of Realizations	1,000
Number of Particles	120,000

3.1.2.1 Selection of Control Planes (Siting Horizons)

It is assumed here that the compliance boundary for the Shoal site will be the regulatory-based contaminant boundary. This boundary relies on using the maximum

contaminant levels (MCLs) for the different radionuclides in determining the size of the contaminant boundary. This boundary is hereafter referred to as the MCL-based contaminant boundary. Using the MCL-based boundary as a compliance boundary, the selection of the control planes or siting horizons is as follows. First, the flow model at Shoal is analyzed to determine the statistical characteristics of the velocities at the site. For each realization, a large number of particles are tracked in the space-time domain and the velocity of the center of mass of the resulting plume is computed for each time step. Then, the average velocity of the center of mass at any time T ($\overline{V}_{c.o.m.}\big|_T$) is obtained by averaging the center of mass velocity from time zero to time T. That is

$$\overline{V}_{c.o.m.}\Big|_T = \frac{1}{N} \sum_{t=\Delta t}^{t=T=N\,\Delta t} \overline{V}_{c.o.m.}\Big|_t \qquad (4)$$

The mean velocity of the center of mass is computed from Equation (4) for T = 100, 200, …, and 1,000 years. This is repeated for all realizations, and the histograms for the velocity distribution at selected times, T = 100, 200, 500, and 1,000 years, are shown in Figure 6. Minor differences exist at different times. The computations are repeated at different times to make sure that the velocity of the plume center of mass does not significantly change with time or distance from the working point. The statistics of the ensembles of velocities are computed and summarized in Table 2. The table displays the velocity quantiles (2.5th percentile, first quartile or 25th percentile, second quartile or median, third quartile or 75th percentile, and 97.5th percentile).

Second, the velocity statistics are used to estimate a distance equivalent to a reaction time of 50 years. It is assumed that a reaction time of 50 years is sufficient to take an action in case a monitoring well detects contaminants approaching the compliance boundary. This reaction time allows for corrective actions before the contaminants reach the compliance boundary. As can be seen from Table 2, the highest velocity (the 97.5th percentile at 400 years) is about 0.00321 m/day. With this velocity, a reaction time of 50 years would require a traveling distance (or a buffer zone) of about 60 m. If the actual velocity of the plume center of mass is slower than the selected 97.5th percentile, the 60-m distance would provide a much longer reaction time than 50 years, which is conservative.

To select the CPs, the mean flow direction is first determined so that the CPs could be oriented normal to the mean flow direction. As stated earlier, for the purpose of detection monitoring, the perpendicular orientation of CPs (relative to the prevailing direction of groundwater flow) is more effective than an oblique configuration. Five CPs are selected and oriented perpendicular to the mean flow direction as shown in Figure 7. The selection of the location of these CPs is aimed at providing the necessary distances for a reaction time of 50 years. The farthest CP (CP #5) passes through the western edge of the MCL-based contaminant boundary which is shown in Figure 7 by the black open circle. CP #4 is located at a distance equivalent to a 50-year reaction time (about 60 m as mentioned above) from the farthest point on the MCL boundary. CP #3 is at a distance of 60 m from CP #5. The next CP (CP #2) passes through the eastern edge of the MCL boundary shown by the black open circle in the figure. The remaining CP (CP #1) is at a distance of 60 m from CP #2. By taking a 50-year reaction time from CP #2, CP #5, and the farthest northeastern point on the MCL boundary, a safeguard is provided against contaminant crossing the compliance boundary

along the mean flow direction (mean plume trajectory) and from either sides of the mean trajectory shown in the figure.

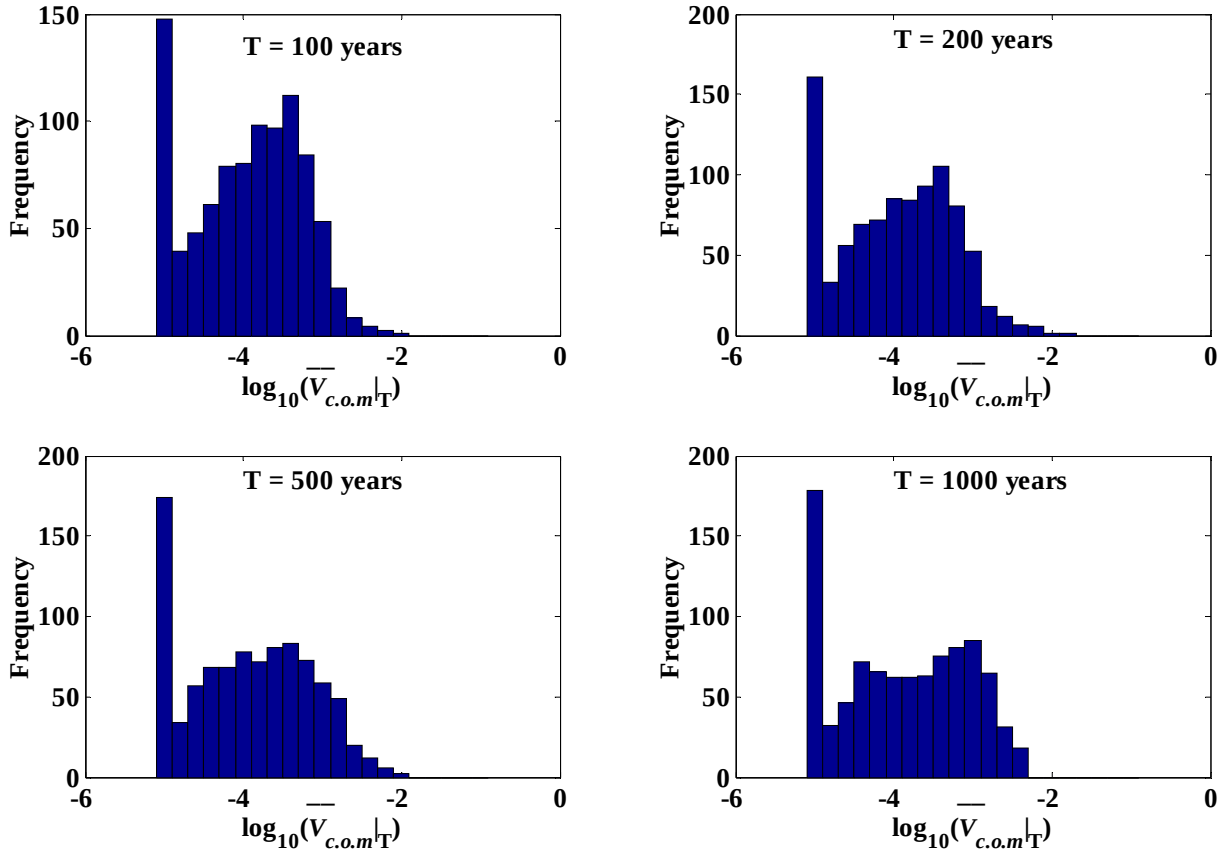

Figure 6. Distribution of Log_{10} of the temporal mean of the center of mass velocity (i.e., mean of c.o.m. velocity at Δt, $2\Delta t$, $3\Delta t$, …, T) with T being 100, 200, 500, and 1,000 years.

Table 2. Center of mass velocity distribution quantiles (2.5th percentile, first quartile, second quartile (median), third quartile, and the 97.5th percentile) in meters per day.

	Velocity Quantiles (m/day)				
Time (years)	2.5th	25th	50th	75th	97.5th
100	1.37E-06	3.16E-05	0.000133	0.000387	0.00163
200	1.18E-06	2.89E-05	0.000124	0.000389	0.002501
300	1.19E-06	2.71E-05	0.00012	0.000413	0.003075
400	1.16E-06	2.61E-05	0.000118	0.00045	0.003209
500	1.12E-06	2.63E-05	0.00012	0.000474	0.003163
600	1.09E-06	2.61E-05	0.000121	0.000514	0.003087
700	1.05E-06	2.54E-05	0.000127	0.000567	0.003065
800	1.02E-06	2.54E-05	0.000128	0.000602	0.003052
900	1.01E-06	2.58E-05	0.000135	0.000629	0.003079
1,000	9.98E-07	2.56E-05	0.00014	0.000671	0.003099

It can be seen from Figure 7 that the five CPs are oriented normal to the flow direction which is not parallel to the model's y-axis. This results in the CPs not being parallel to the model's x-axis. However, to facilitate some of the subsequent computations and analyses, a rotated coordinate system (x', y') is used and some of the distances and positions in the results are presented using this rotated coordinate system. Thus, a distinction will be made between the model coordinates and these rotated coordinates. Model coordinates are denoted as x and y, whereas the rotated coordinates are denoted as x' and y'. Figure 8 shows the model domain and model coordinate system in relation to the rotated coordinate system and the five CPs.

3.1.2.2 Transport Analysis for the Five Control Planes

The transport simulation layout is shown schematically in Figures 9 and 10. Figure 9 shows a three-dimensional view of the simulation domain, the cavity location, and five CPs located as described above. The figure also shows a zoom-in view showing the source and the five CPs, with the y'-axis scale exaggerated to clearly show the five CPs. A plan view is also presented to show the numbering sequence of the CPs, which will help in tying the results to this schematic picture.

Transport simulations are conducted for the 1,000-year regulatory time frame. The particles representing the radionuclide source are tracked in the space-time domain for the total simulation time of 1,000 years. At every time step and for each CP, the dimensions of the plume as it crosses a particular CP are obtained and recorded. Figure 10 shows how the plume width, height, and centroid (or center of mass) location are obtained for a certain CP. Therefore, for each CP, the plume width, height, and (x', z) coordinates of the plume center of mass are recorded for every time step. This output is subsequently analyzed at times 100, 200, 500, and 1,000 years after detonation. For any of these four times, the maximum plume width and the maximum plume height that were ever attained from time zero until this time are selected for plotting the histograms discussed shortly. For the center of mass of the plume as it crosses the different CPs, the average value of the center-of-mass location is obtained by averaging the non-zero values from time zero to the current time. The zero values of the center of mass of the plume result when no particles exist in the vicinity of the CP at the current time step. This occurs due to the dispersion of particles and the fact that they do not migrate in a continuous manner.

Before applying Hudak's (1994) approach to Shoal using these transport simulations, it is of interest to analyze the results and gain some understanding of how the flow system behaves at the site and how transport occurs. Figure 11 shows the distribution of the percentage of total mass crossing each of the five CPs at different times. The number of realizations with mass crossing the control plane for each case is donated as N_{tot}. Figure 11 shows that after 100 years from detonation, 66 realizations (out of 1,000) had mass arriving at CP #1, and the fastest migration rate among these realizations led to about 35 percent breakthrough. However, only 36 realizations crossed CP #5 with a maximum of about 17 percent mass breakthrough. After 1,000 years, 765 realizations showed breakthrough values at CP #1, whereas the number of realizations showing breakthrough values at CP #5 becomes 670 with a maximum mass arrival of 100 percent in both cases. These results are based on ignoring matrix diffusion, and no radioactive decay is considered. These results are also based on those radionuclides with no or insignificant surface deposits (e.g., tritium and carbon-14).

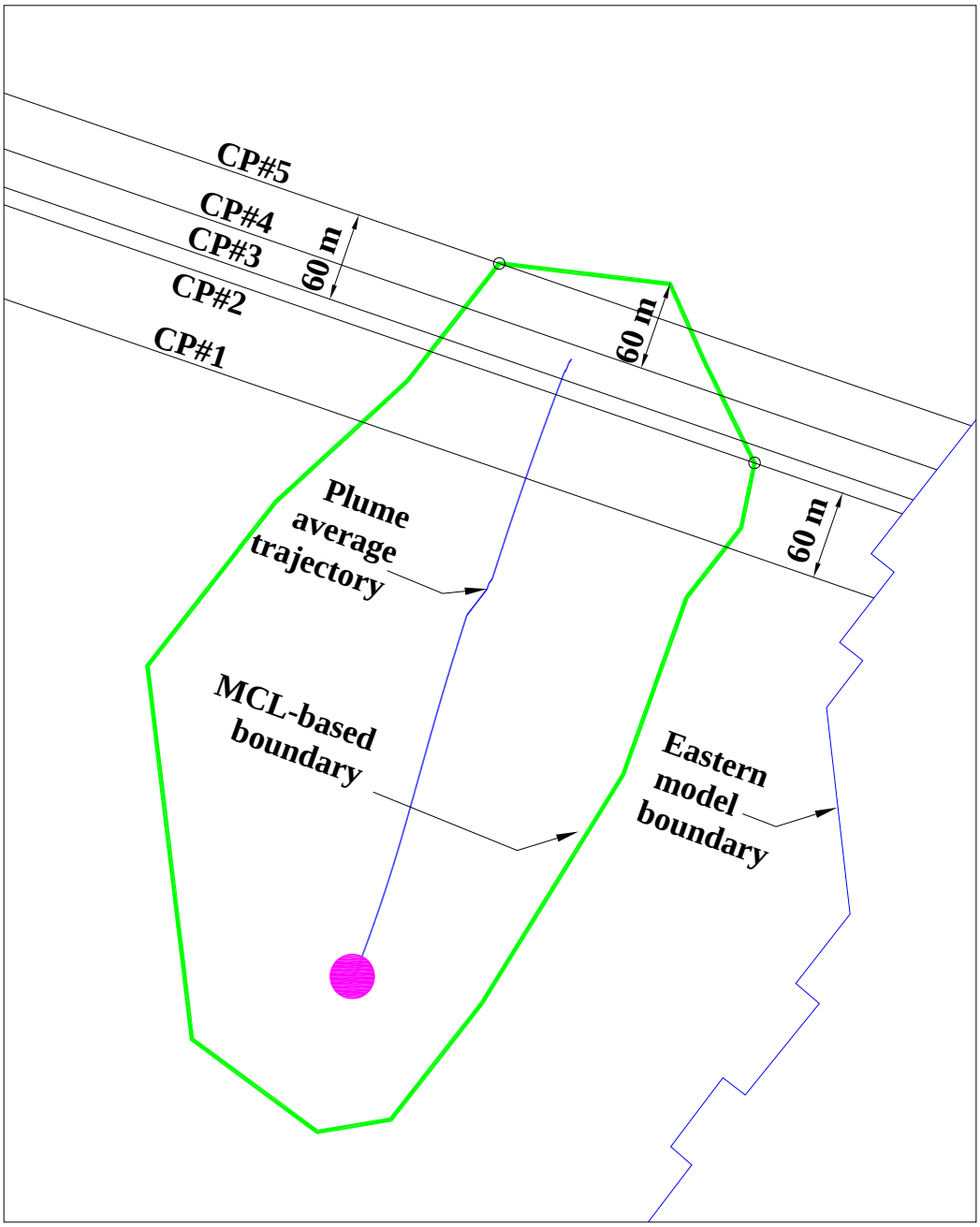

Figure 7. Selection of control plane location and orientation normal to the mean flow direction.

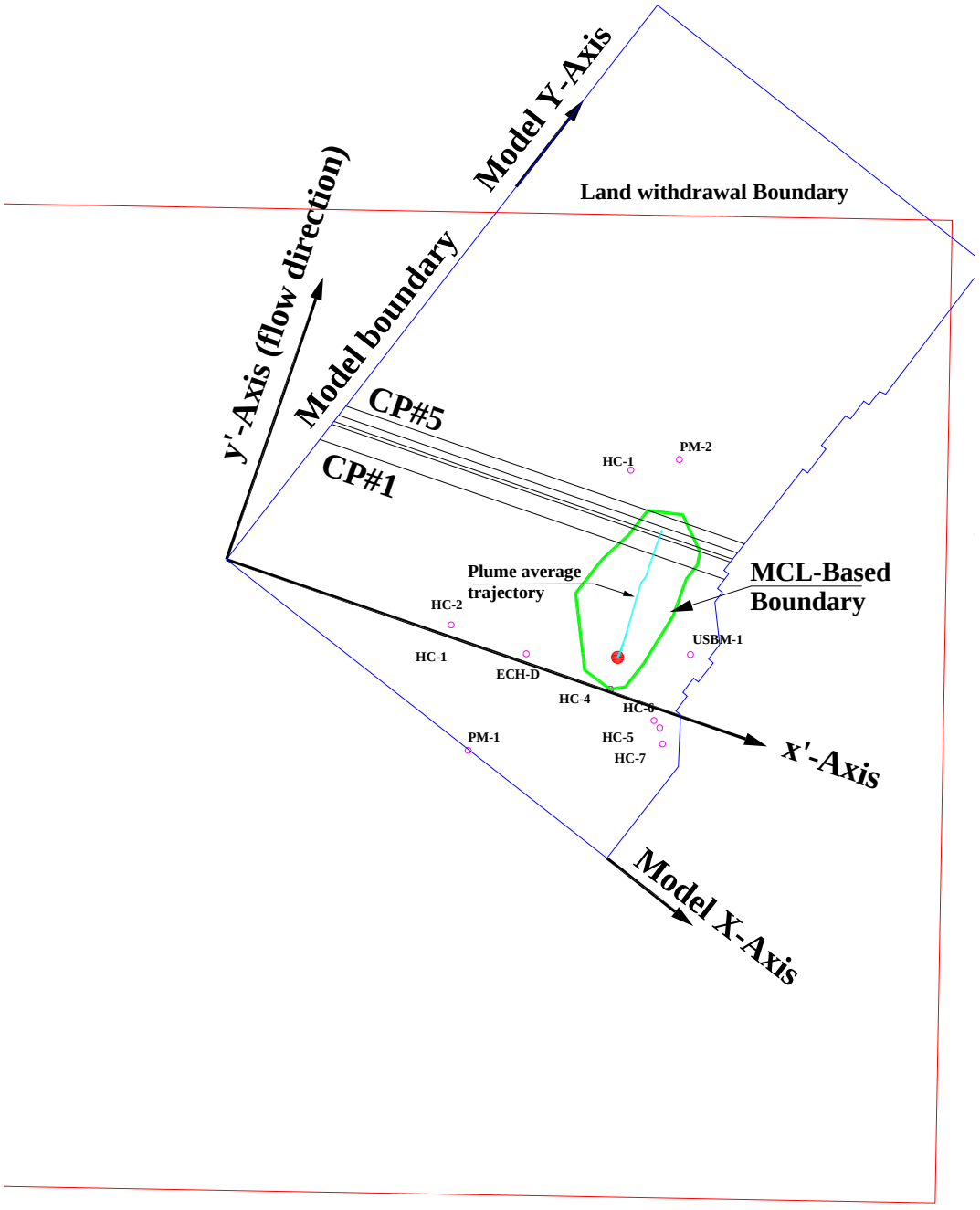

Figure 8. Original model coordinates (x, y) and rotated coordinates (x', y') relative to the MCL-boundary. Locations of the five control planes are also shown.

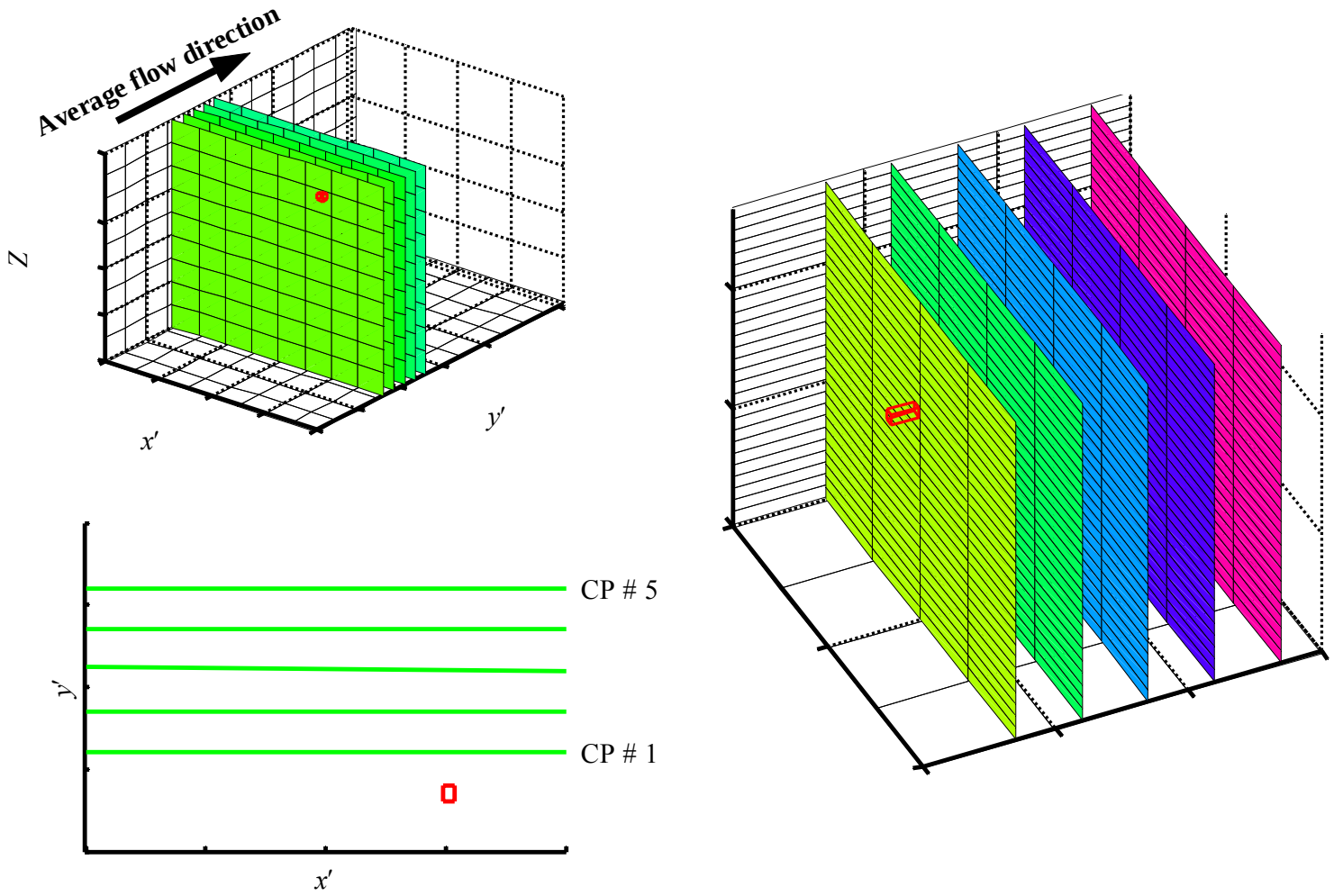

Figure 9. A schematic three-dimensional view (top) showing the model domain, the cavity and the five CPs (CP #1 through CP #5), a zoom-in around the cavity and the CPs (right - exaggerated scale in the *y′*-direction to allow distinction between control planes), and a two-dimensional plan view showing the location of the five CPs relative to the cavity.

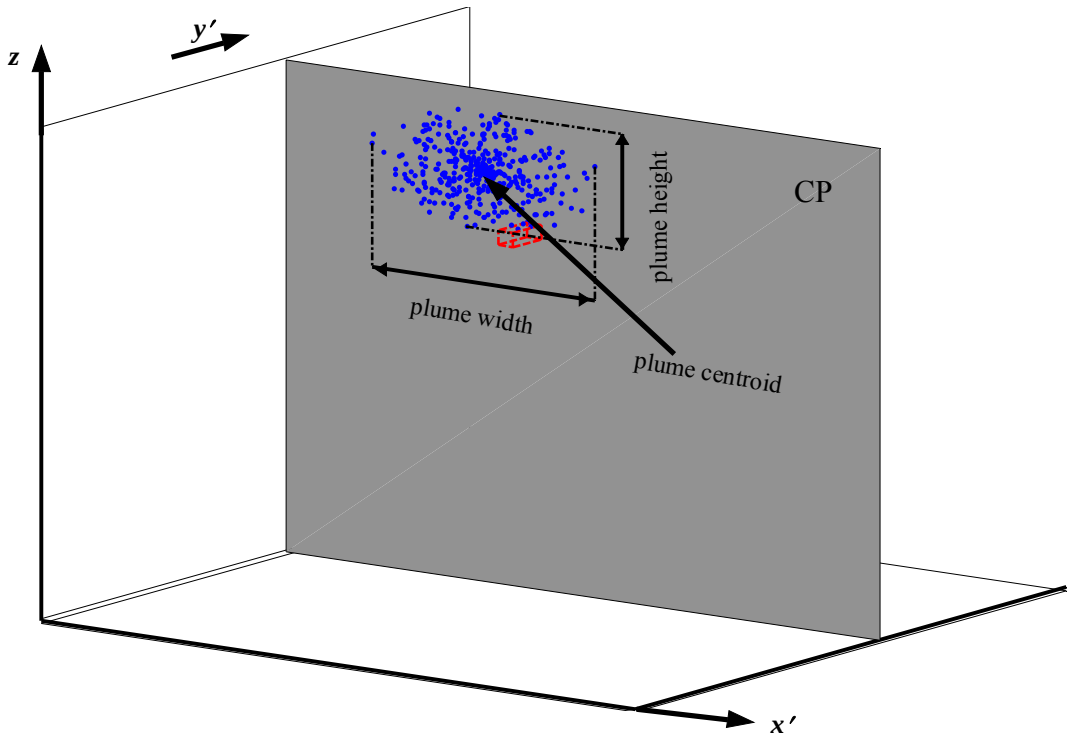

Figure 10. Schematic representation of the plume width and height as particles cross the CP.

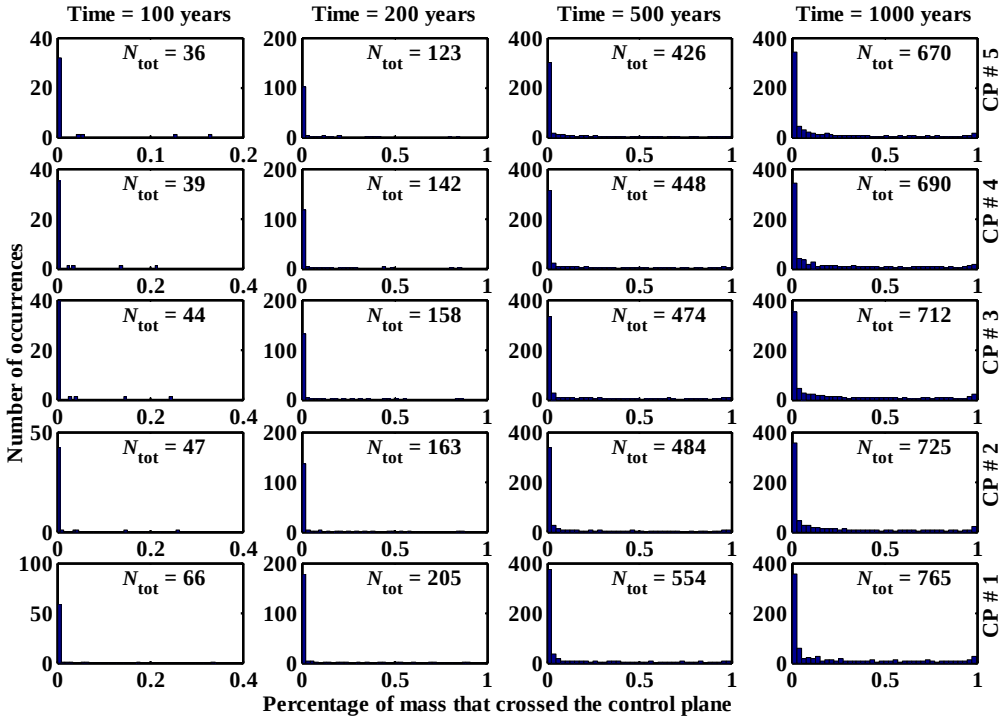

Figure 11. Distribution of the total mass crossing CP #1 through CP #5 at different times.

Based on these results, it can be seen that there is a possibility for plume migration away from the Shoal cavity. However, the actual migration distances after accounting for all retardation mechanisms is small as shown in the contaminant boundary report (Pohll and Pohlmann, 2004). The farther away one gets from the working point the lower the likelihood of migration (and thus detection) becomes.

Figures 12 and 13 display the distribution of the plume width and plume height as defined in Figure 10 for the different times and the different CPs. The results of Figure 12 indicate that in all cases, the average plume width over all realizations showing mass arrival does not exceed 470 m. Also at the 95 percent confidence level, the upper bound or the 97.5 percent prediction quantile (PQ) of the plume width at all CPs is about 1,280 m. Figure 13 shows that the average plume height does not also exceed 444 m with an upper PQ of about 1,102 m. With the fractured nature of the granite formation at Shoal, the actual width and height of the plume may in fact be smaller than predicted by the model. This is because the model applies a continuum approach to this problem and for realizations involving flow through fractured systems, this may overestimate dispersion.

Figures 14 and 15 show the distribution of the x'- and z-locations of the plume center of mass when it crosses the CPs. The figures show that the center of mass in many realizations is around $x' = 1{,}300$ m from the domain origin with some skewness in the distribution of x' toward the smaller values (e.g., closer to the domain origin). It should be remembered that the distances used to obtain x' are measured in the rotated coordinate system (see Figure 8). In the vertical z-direction, the plume center of mass has a left-skewed distribution (toward lower elevations) with a maximum of about 1,200 m, which coincides with the bottom edge of the source representing the test cavity.

The distribution in the vertical z-direction provides a guidance of where to sample the monitoring well for concentration measurements. It should be mentioned that the variability of the z-location between realizations is partly a result of the uncertainty in the recharge and conductivity values impacting the flow direction and the elevation at which migration occurs in the northeastern direction. Therefore, it is important to account for the variability in the z-direction by, for example, sampling at multiple elevations but with emphasis on the intervals likely to encounter radionuclide migration as predicted by the model.

The results indicate that the location likely to encounter plume migration is along a line that deviates from the longitudinal centerline of the domain downstream of the cavity. This deviation is apparent by looking at the mean flow direction depicted in Figure 8, which dictated the use of the rotated system to have the mean flow direction parallel to the rotated y'-axis. For this reason, potential well locations are selected to be aligned along a line that deviates from the longitudinal centerline of the model domain and matches the mean flow direction.

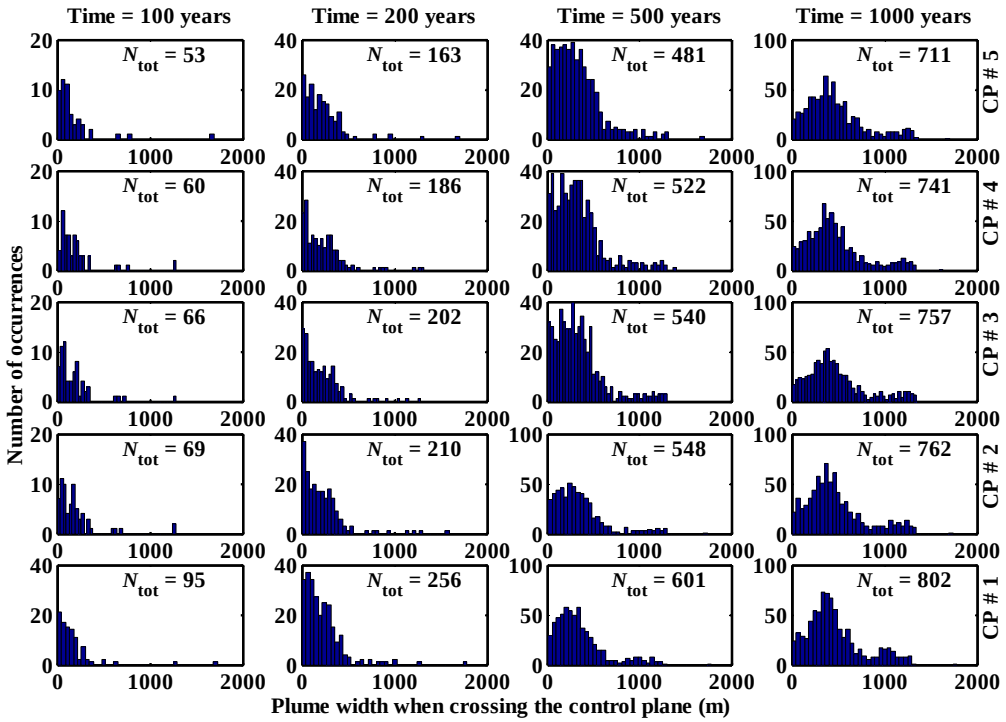

Figure 12. Distribution of plume width as it crosses CP #1 through CP #5 at different times.

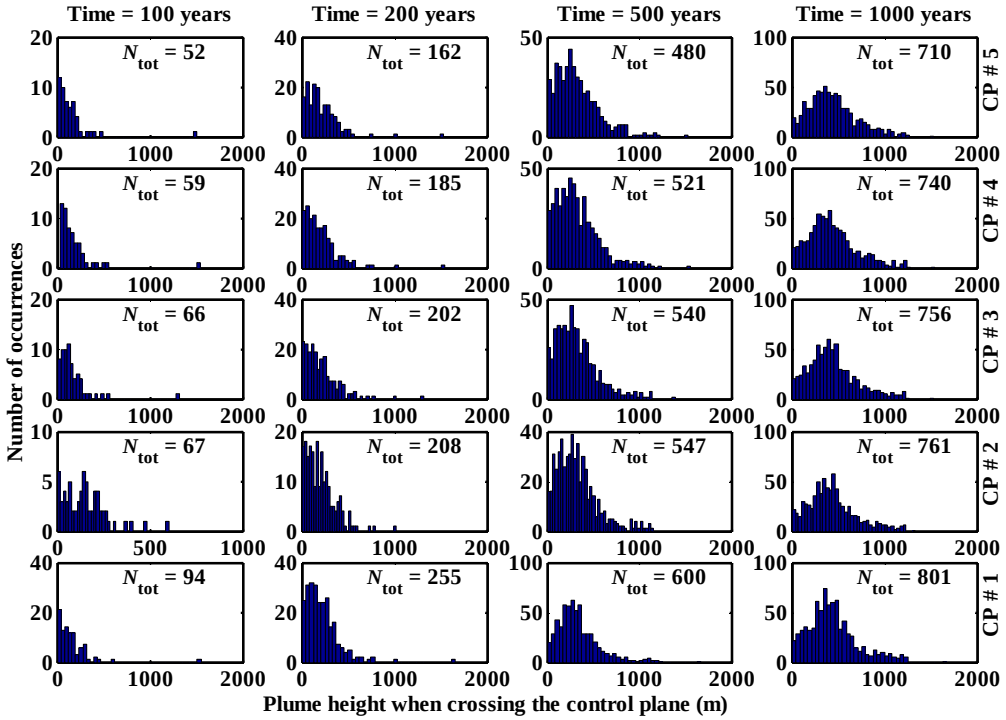

Figure 13. Distribution of plume height as it crosses CP #1 through CP #5 at different times.

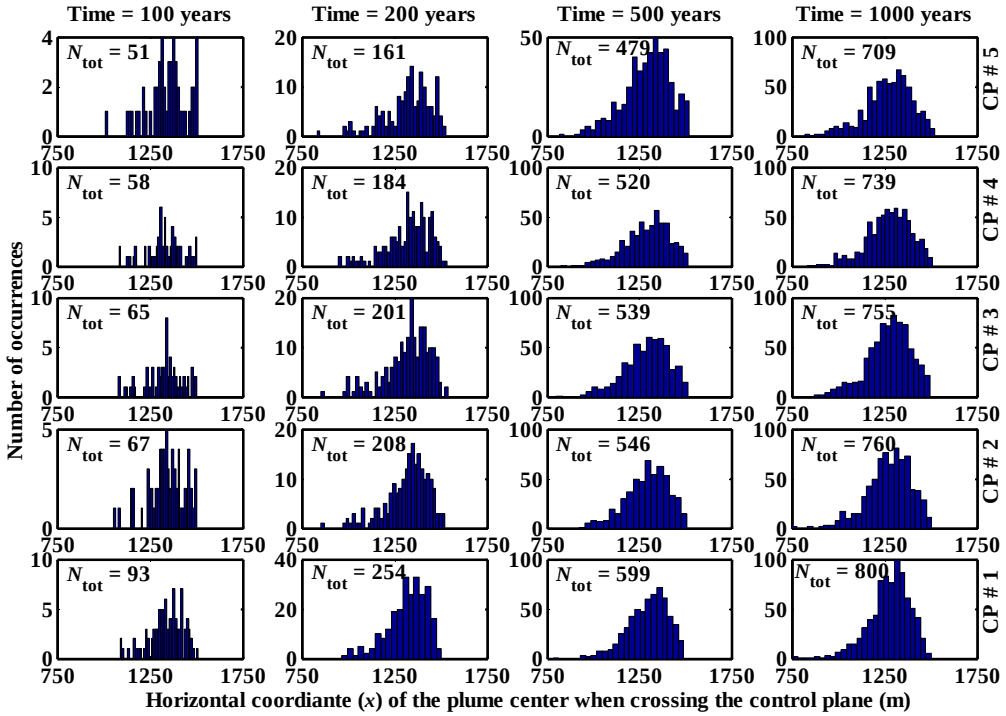

Figure 14. Distribution of the x'-location of the plume center of mass when crossing CP #1 through CP #5 as average values from time zero to the given times.

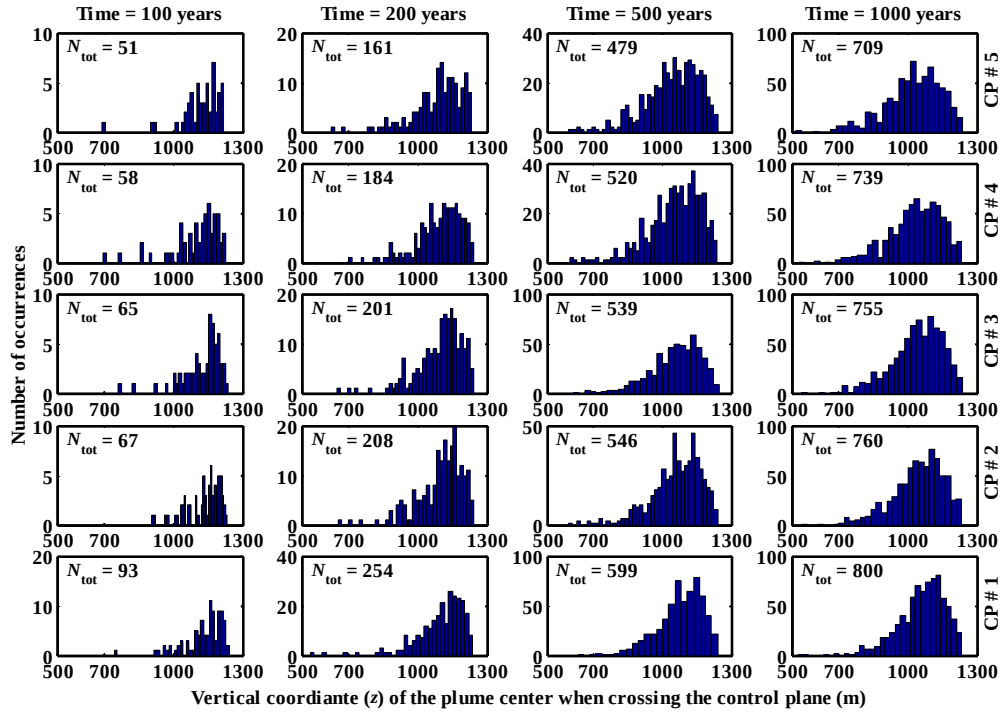

Figure 15. Distribution of the z-location of the plume center of mass when crossing CP #1 through CP #5 as average values from time zero to the given times.

3.1.3 Application of First Tool to Shoal

To apply Hudak's (1994) approach to Shoal for the purpose of determining the minimum number of wells, N_i, needed to span a siting horizon (or a control plane), S_i and W_i are obtained as discussed earlier. To obtain the maximum well spacing, S_i, the simulation results for the five CPs where the plume width at each CP is reported for each realization of the stochastic flow and transport model at Shoal are analyzed. To summarize the results for the different times, different CPs, and different realizations, Table 3 presents the PQ obtained from the 1,000 realizations of plume widths. For these Monte Carlo realizations, the PQs are computed by ranking the 1,000 plume widths. Then, for a 95 percent confidence interval, the realization ranked number 25 is used as a lower bound (2.5 percent PQ), realization number 975 as an upper bound (97.5 percent PQ), and the average of realizations 500 and 501 as the median or 50 percent PQ. It should be mentioned here that the plume widths are computed along the control plane in x'-direction, which is the rotated axis, not the model axis.

Because some of the plume realizations have very short migration distances and thus these plumes did not cross some or all of the CPs, the plume widths in these realizations are zeros. Those realizations are eliminated from the 1,000 Monte Carlo realizations before ranking. The remaining non-zero-width plumes are ranked and the different PQs are obtained by adjusting the realization number to be picked based on the total number of non-zero-width plumes. Given the results shown in Table 3, it can be seen that on average, the plume width barely exceeded 400 m at 1,000 years. At 100 years, however, the plume width is about 120 m on average. For each CP and for each time considered, the parameter S_i is obtained as the 50-percent PQ of the plume width as it crosses the CPs.

Table 3. Prediction quantiles (PQ) for the plume width at different times and for the five CPs.

	Plume width when crossing the CP (m)											
Control	t = 100 years			t = 200 years			t = 500 years			t = 1,000 years		
Plane	2.5% PQ	50% PQ	97.5% PQ	2.5% PQ	50% PQ	97.5% PQ	2.5% PQ	50% PQ	97.5% PQ	2.5% PQ	50% PQ	97.5% PQ
CP #1	5.1	114.5	628.8	6.6	174.2	828.7	26.0	288.8	1112.2	41.9	402.0	1200.6
CP #2	11.2	137.8	697.5	11.4	172.3	809.3	27.2	287.7	1159.7	43.2	400.8	1248.7
CP #3	3.0	127.9	650.3	10.3	165.5	802.7	17.7	293.5	1153.5	40.7	402.4	1255.9
CP #4	15.0	129.5	1279.8	10.3	178.2	861.9	21.0	290.4	1134.2	37.4	408.2	1251.7
CP #5	0.0	104.5	778.1	10.2	179.0	788.2	21.4	287.1	1048.8	36.1	406.9	1255.3

The zone of potential contaminant migration, W_i, for each CP and at each time considered is obtained by analyzing the distribution of the x'-coordinate of the plume center of mass as it crosses the CPs. Table 4 displays the PQs for the x'-position of the center of mass of the plume. To obtain the parameter W_i, the difference between the 97.5 percent PQ (representing the upper bound or the farthest plume to the southeast direction) and the 2.5 percent PQ (representing the lower bound or the farthest plume to the northwest direction) is computed and taken as a representation of the zone of potential migration.

After determining the two parameters S_i and W_i for all CPs, the CP detection efficiency, S_i/W_i is determined and Equation (1) is used to obtain the minimum number of wells needed for each CP. Table 5 shows the values of S_i, W_i, S_i/W_i, and N_i for each CP and all times considered. In general, CP #5 tends to have the lowest efficiency (smallest S_i/W_i ratio) and CP #1 tends to have the highest efficiency, but this is not consistent through time and the efficiencies of the various CPs are often very similar. From Table 5, it seems that CP #1 is slightly favored, though wells on the other CPs (particularly CP #2 and #4) offer similar efficiency.

Table 4. Prediction quantiles (PQ) for the x'-position of the plume center of mass at different times and for the five CPs.

Horizontal coordinate x' of the plume center of mass when crossing the CP (m)												
Control	t = 100 years			t = 200 years			t = 500 years			t = 1,000 years		
Plane	2.5% PQ	50% PQ	97.5% PQ	2.5% PQ	50% PQ	97.5% PQ	2.5% PQ	50% PQ	97.5% PQ	2.5% PQ	50% PQ	97.5% PQ
CP #1	1093.5	1348.5	1472.6	1025.2	1332	1466	1018.1	1311.8	1464.5	938.7	1290.3	1453.5
CP #2	1086	1344.1	1489.9	1022.2	1340.9	1492.3	989.7	1303.1	1478.1	949.9	1283.7	1464.2
CP #3	1079.8	1339.2	1492.4	1000.1	1344.7	1482.5	980.3	1304.3	1480.9	956	1283.8	1467.1
CP #4	1082.6	1326.3	1503.1	1009.5	1343	1492.7	989.5	1305.7	1489.4	968.1	1285.5	1473
CP #5	1012.4	1358.1	1506.4	1004.9	1338.7	1499.7	976.5	1311.5	1504	935.3	1285.4	1483

Table 5. Parameters of Equation (1), the resulting CP efficiency (S_i/W_i), and the minimum number of wells, N_i, to span each CP at different times.

S_i, W_i, siting horizon efficiency (S_i/W_i), and N_i for the five CPs and the different times																
Control	t = 100 years				t = 200 years				t = 500 years				t = 1,000 years			
Plane	S_i	W_i	S_i/W_i	N_i	S_i	W_i	S_i/W_i	N_i	S_i	W_i	S_i/W_i	N_i	S_i	W_i	S_i/W_i	N_i
CP #1	114.5	379.1	0.30	3	174.2	440.8	0.40	2	288.8	446.4	0.65	1	402.0	514.8	0.78	1
CP #2	137.8	403.9	0.34	2	172.3	470.1	0.37	2	287.7	488.4	0.59	1	400.8	514.3	0.78	1
CP #3	127.9	412.6	0.31	3	165.5	482.4	0.34	2	293.5	500.6	0.59	1	402.4	511.1	0.79	1
CP #4	129.5	420.5	0.31	3	178.2	483.2	0.37	2	290.4	499.9	0.58	1	408.2	504.9	0.81	1
CP #5	104.5	494.0	0.21	4	179.0	494.8	0.36	2	287.1	527.5	0.54	1	406.9	547.7	0.74	1

In continuum porous media, detection efficiency may increase as distance downgradient from the source increases. This is because plume spreading due to heterogeneities may be larger than plume meandering (variability in the plume trajectory from the ambient groundwater flow direction). This is likely to occur if the size of the initial plume is larger than the characteristic length of heterogeneity (e.g., conductivity correlation scale). In this case, the potential zone of contaminant migration increases at a slower rate than the plume size, which results in increasing detection efficiency as distance downgradient increases. The analysis at Shoal showed the opposite trend. The opposite trend is found to be attributed to the fractured system modeled and the fact that each plume moves in a set of connected fractures with high velocities and little dispersion. On the other hand, the variability in the fracture networks from one realization to the next leads to a faster rate of increase in the potential migration zone compared to the rate of plume growth.

It can also be seen from Table 5 that the required number of wells is generally between one and two. Only at t = 100 does the analysis suggest a need for three or four wells, and this is a result of very narrow plumes (e.g., few fast particles) reaching CP #4 and CP #5 at 100 years, leading to a small S_i value and in turn a large number N_i of required wells. Based on these results, it is reasonable to assume that two wells at any single siting horizon or CP will have a good chance of detecting the plume migration if it reaches to that particular CP. Therefore, in all subsequent analysis, it is assumed that the monitoring network at Shoal will not have more than two wells along any single siting horizon or CP. This is also consistent with the fact that the Shoal flow model still needs to be validated.

3.2 Second Design Tool

The second set of analyses performed for designing the long-term monitoring network at Shoal is similar to the analysis performed for CNTA (Hassan, 2003), and is based on using the hydrogeologic approach combined with the simulation and probability based approaches to select the set of monitoring wells that will serve two purposes. The first objective is to place

wells in locations likely to encounter fast migration pathways, thus using these wells in the long-term monitoring of the site. The second, short-term objective is the collection of data for the validation of the groundwater flow and transport model. The selection criteria may be tailored to meet this objective and facilitate the collection of the most relevant data from the most important locations for evaluating the different model components. By keeping in mind that the long-term monitoring wells can also serve the validation purpose, the benefit from these wells is maximized and an efficient long-term monitoring program can be developed for site closure.

3.2.1 Approach Summary

The details of the simulation-probabilistic approach are presented in Hassan (2003). Here, the approach is briefly summarized and the application to Shoal is described in detail. It is assumed that a monitoring well fails if (1) an arbitrary percentage (e.g., 2 percent) of the plume mass crosses a CP that is passing through the well and located normal to the mean flow direction, and (2) the well does not detect the presence of contaminants. It is important to note that the "arbitrary percentage" is an important value that can be negotiated. Using the multiplication rule of the conditional probability theory, one can define the probability of failure in year t for a monitoring well located at $\mathbf{x}_j = (x_j, y_j, z_j)$, as

$$P_f(t;\mathbf{x}_{jk}) = P\left(\frac{1}{M_{total}}\int_0^t Q(\tau;x_k)\,d\tau \geq \alpha\right)\left(1-P_{dj}\right) \qquad (5)$$

where $P_f(t;\mathbf{x}_{jk})$ is probability that the well located at $\mathbf{x}_j$ will not detect the plume when α percent of its mass crosses the CP located at distance x_k from the center of the source along the mean flow direction (to the northeast for the Shoal model) in a time frame less than or equal to t years, $\int_0^t Q(\tau;x_k)\,d\tau$ is the cumulative mass arrival to the CP located at x_k, M_{total} is the total mass of contaminant available in the aqueous phase, and P_{dj} is the probability of detection by the monitoring well located at $\mathbf{x}_j$. An analogous definition is

$$P_s(t;\mathbf{x}_{jk}) = P\left(\frac{1}{M_{total}}\int_0^t Q(\tau;x_k)\,d\tau \leq \alpha\right) P_{dj} \qquad (6)$$

where $P_s(t;\mathbf{x}_{jk})$ is the success probability, that is, the probability that the monitoring well will detect the plume in year t if α percent of its total mass or less arrives at the CP of the monitoring well by year t. It can be seen that for individual wells, the time-dependent probability of failure and probability of success are zero at early times and then they both start to increase when the plume reaches the CP where the well is located. If a certain percentage of the plume mass crosses the CP before the monitoring well detects any contaminants, P_{dj} is zero and the success probability is zero. If the well detects contaminants before α percent of the mass crosses the CP, then P_{dj} is 1.0 and the failure probability becomes zero. This binary decision point provides a tangible measure of success, which can be expanded to multiple wells.

The value of P_{dj} can be determined from the plume migration analysis. A plume will be detected by a monitoring system only if the groundwater flow lines passing through the source also pass through the screened interval of the monitoring well (Massmann and Freeze, 1987a). Plume intersection along the well sampling intervals will lead to contaminant detection. This probability of detection by a monitoring well can be determined from Monte Carlo simulations. The detection occurs when particles representing the contaminant mass (using a particle-tracking

approach for modeling the transport processes) pass through any of the vertical cells where the well is located. However, to account for the temporal aspect, to overcome the issue of the classified initial source mass, and to allow for comparing different well locations, the area of the *t-z* distribution of the normalized masses (particle masses) for a monitoring well is used as an indicator of the likelihood of detection. Thus the detection probability for a monitoring well *j* can be obtained using Monte Carlo simulation as

$$P_{dj} = \sum_{i=1}^{NMC} \frac{W_{ji}}{NMC} \tag{7}$$

where *NMC* is the number of Monte Carlo realizations used in the analysis and W_{ji} can be obtained as

$$W_{ji} = \int_0^t \int_{z=z_b}^{z=z_t} M_{ji}(\tau, z)\, dz\, d\tau \tag{8}$$

where $M_{ji}(\tau, z)$ is the resident mass in the monitoring well cell located at elevation z and time τ, z_b is the bottom elevation of the lowest cell that can be sampled by the well, and z_t is the top elevation of the uppermost cell that can be sampled.

The implementation of the above analysis is done through the following steps (see Figure 16). The first step is to identify the possible candidate locations, *J*, for the monitoring wells. The exact location will be determined with this analysis where the different candidate locations of different wells are compared and the optimal location with highest success probability (lowest failure probability) is chosen. The second step is to select a time frame for the analysis, which is represented by the simulation time scale, *T*, and the time, *t*, at which probabilities are to be obtained.

The third step is to run Monte Carlo simulations and record for each realization the *t-z* distribution of the resident mass ($M_{ji}(\tau, z)$ in Equation (8)) within the cells occupied by each monitoring well. The integration of this mass distribution gives W_{ji} for each realization $i = 1$ to *NMC* and each well *j*. The fourth step is to compute for each candidate well location the probability that α percent of the total plume mass crosses the CP, *k*, passing through that location in time *t* or less. This can simply be obtained by integrating the total mass flux breakthrough curve for each CP ($k = 1, \ldots K$ with $K \le J$) from time zero to time *t*. The fifth step is to use Equation (6) to compute the success probability for each candidate well location (due to the computational burden, only a finite number of candidate locations will be evaluated). The locations with the highest success probability will then be selected as potential well locations.

Although computationally demanding, the approach described above is simple in nature and relies on the simulation approach combined with the hydrogeologic expertise and knowledge about the site. A number of reasons lead to the use of this simplified design approach as opposed to the automated optimization techniques. First, the underlying model structure is generally uncertain to justify an elaborate search for "optimal" designs that may actually be no better than *ad hoc* strategies proposed based on familiarity with the site. Second, the optimization approaches are sought in cases of designing a monitoring network that consists of many wells and the question becomes where the optimum locations are for these wells. For the Shoal site, the depth of the wells limits the number that can be drilled, as compared to more common, and shallow, hazardous waste sites. Simple approaches lead to clear and easy choices for Shoal and yield results similar to more complicated optimization approaches.

3.2.2 Application of Second Tool to Shoal

Having analyzed the results of the particle tracking model for the selected CPs or monitoring horizons, the steps illustrated in the flowchart of Figure 16 can now be implemented. Fifteen candidate locations are selected along the five CPs (CP #1 through CP #5) with three potential well locations assigned to each CP. The central well coincides with the average plume trajectory. The edge wells are located such that they enclose 50 percent of the plume trajectories at each CP. The locations of these edge wells are determined from the analysis of the histograms of the plume center of mass position, x', as it crosses each CP. The locations of the resulting 15 wells are shown in Figure 17. These 15 wells in addition to HC-1 and HC-4 will be analyzed as potential monitoring wells for the purpose of selecting a three-well network with high detection efficiency (using the third tool).

In addition, a new three-well network will be analyzed and compared to the results of the individual networks formed from the 17 wells mentioned above. This network is obtained by drawing a new boundary inside the MCL-based contaminant boundary at a perpendicular distance (an offset) of about 60 m (i.e., equivalent to a 50-year reaction time) and locating three wells at the eastern, northeastern, and western edges of this new boundary. This is shown in Figure 18 with the three wells in red circles, denoted as NW1, NW2, and NW3.

The total simulation time is selected as the regulatory time frame of 1,000 years and the time for computing probabilities is selected at the same four times analyzed earlier (100, 200, 500, and 1,000 years). The parameter α is varied between 0.5 percent and 4 percent of the total initial source mass with increments of 0.5 percent. Recall that for a well to be successful in detecting a plume, it has to detect the presence of contaminants when or before a percentage mass of value α crosses the control plane. Since this value is somewhat arbitrary, the analysis is presented for the above-mentioned eight α values. Under these parameter values, the transport simulations are conducted for 1,000 years and total mass flux breakthrough, $Q(t, x_k)$, are computed for each CP ($k = 1, \ldots, 5$). In addition, at each potential well location the resident mass, $M_{ji}(t, z)$, that exists within a certain vicinity of the well ($\Delta x \times \Delta y$) is monitored and saved for each time step and at all elevations.

As an example, Figure 19 shows the t-z distributions of the $\log_{10}$ of the resident mass for each of the 20 potential well locations (wells 1 through 15, HC-1, HC-4, NW1, NW2, and NW3). It is important to note the different color bars and different peak values on these bars. If one integrates these masses along the vertical z-direction, the results can be plotted as in Figure 20. This figure shows the mean value (across all realizations) of this vertically integrated resident mass as a function of time. As can be seen from the figure, the average resident mass does not exhibit any particular pattern. This is because the amount of mass approaching a certain well location depends on the set of fractures and how many realizations have fractures intersecting a well.

The next step in the analysis is to compute the weights, W_{ji}, for each well, j, according to Equation (8). These weights represent vertical and temporal integration (from time zero to t) of the resident mass. These steps are then repeated for each of the 1,000 realizations considered for the Shoal model. The next step according to the flowchart of Figure 16 is to compute P_{dj} for each of the potential well locations according to Equation (7). Figure 21 displays the values of P_{dj} at different times (t = 100, 200, 500, and 1,000 years). It is to be noted that P_{dj} represents the probability that well j detects the plume. Whether this detection is successful or not is computed

by a different term. In other words, if the well detects a plume but after a large portion of it has crossed the CP, that well will have a low success probability.

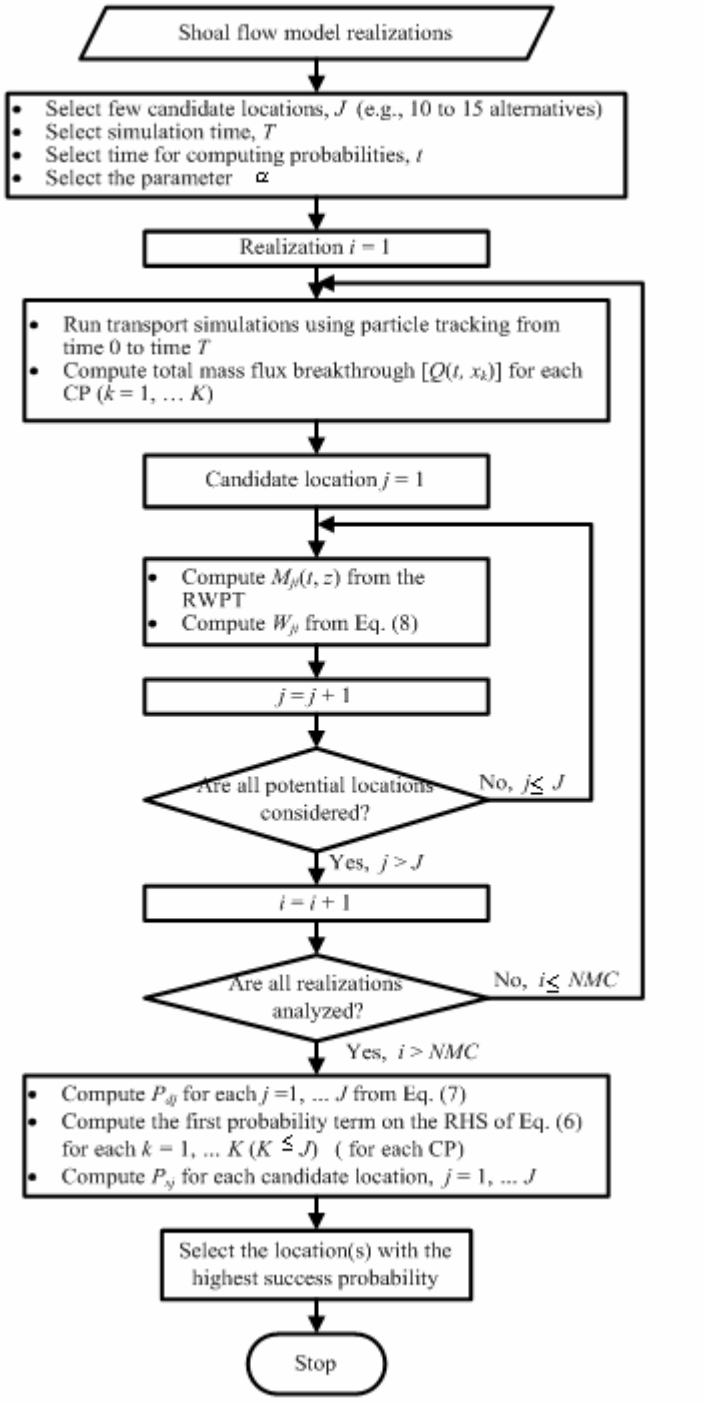

Figure 16. A step-by-step description of the design methodology developed in Hassan (2003) and applied to Shoal as one of the tools used for the design of the monitoring network.

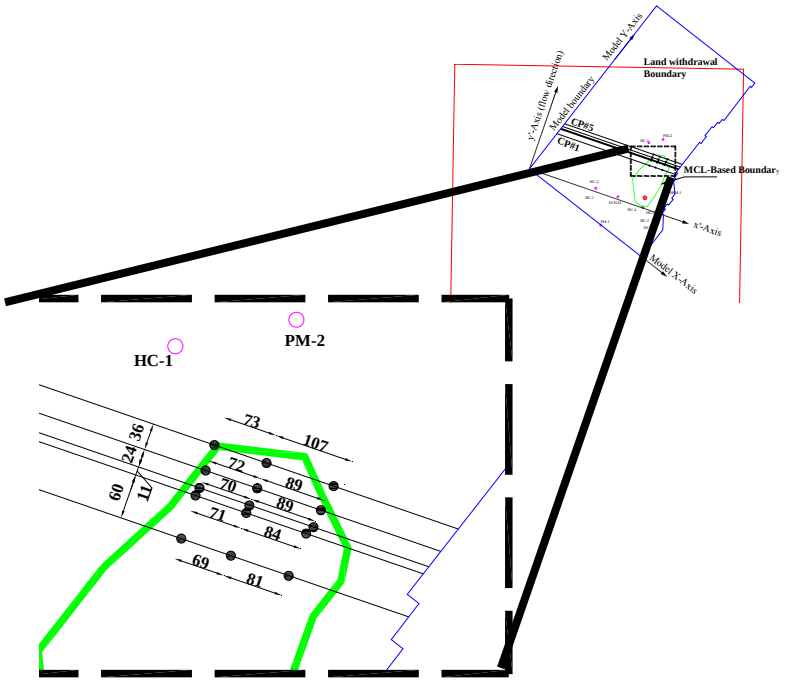

Figure 17. A plan view showing the location of the 15 potential wells and the five CPs relative to the MCL-based boundary.

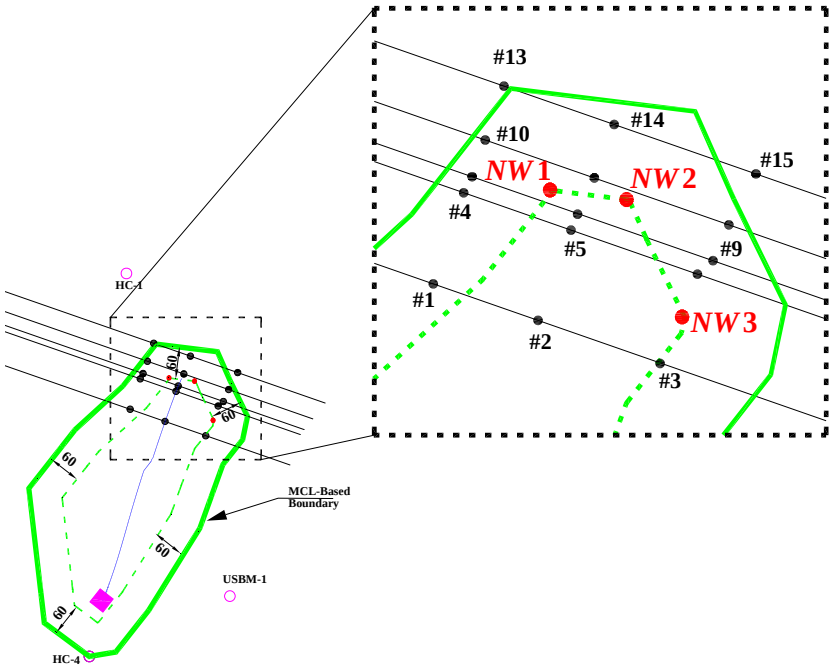

Figure 18. A plan view showing the location of the 15 potential wells (black circles) and the three new wells NW1, NW2, and NW3 (red circles) relative to the MCL-based boundary.

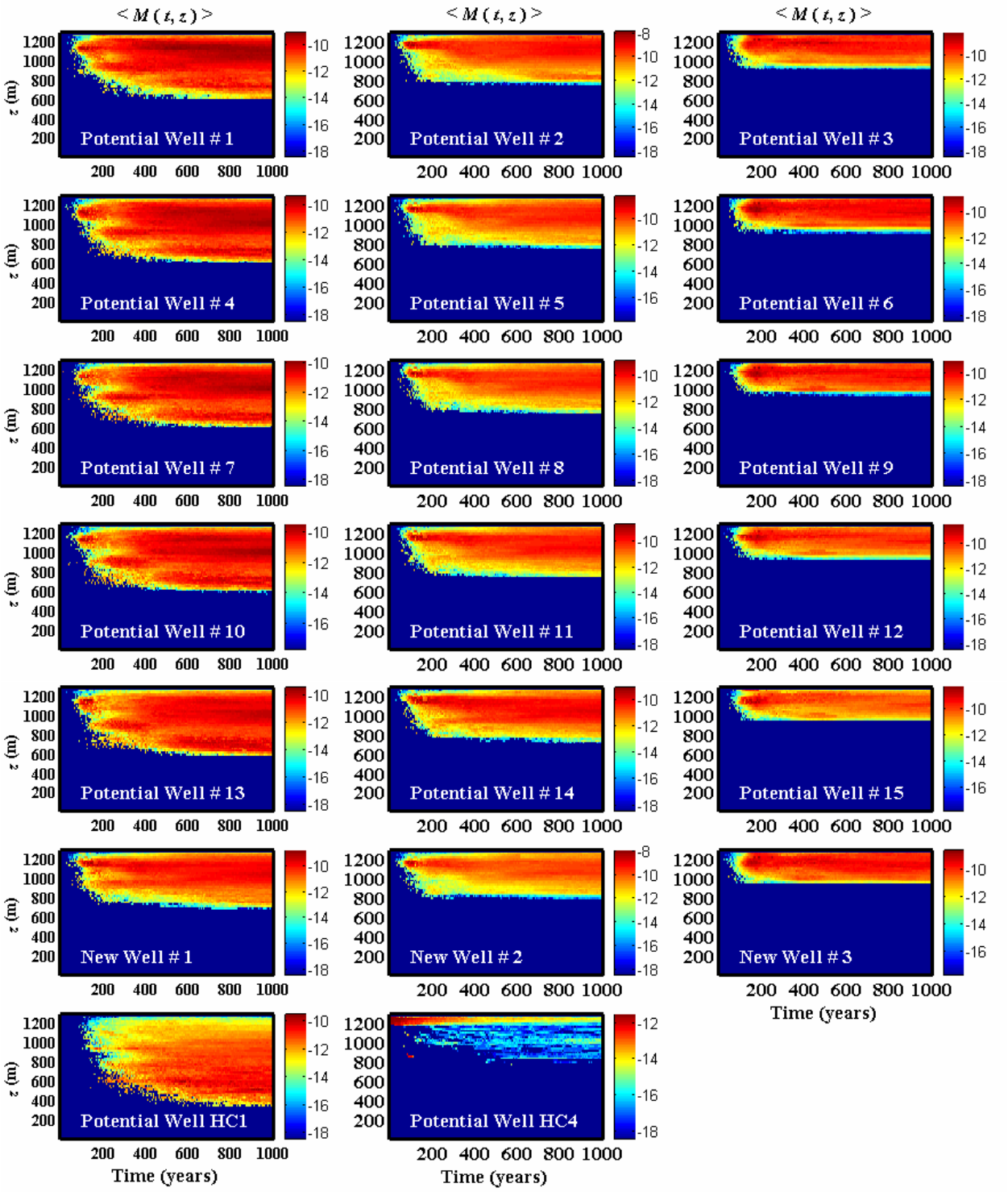

Figure 19. The *t-z* distribution of the resident mass in the vicinity of each of 20 potential well locations.

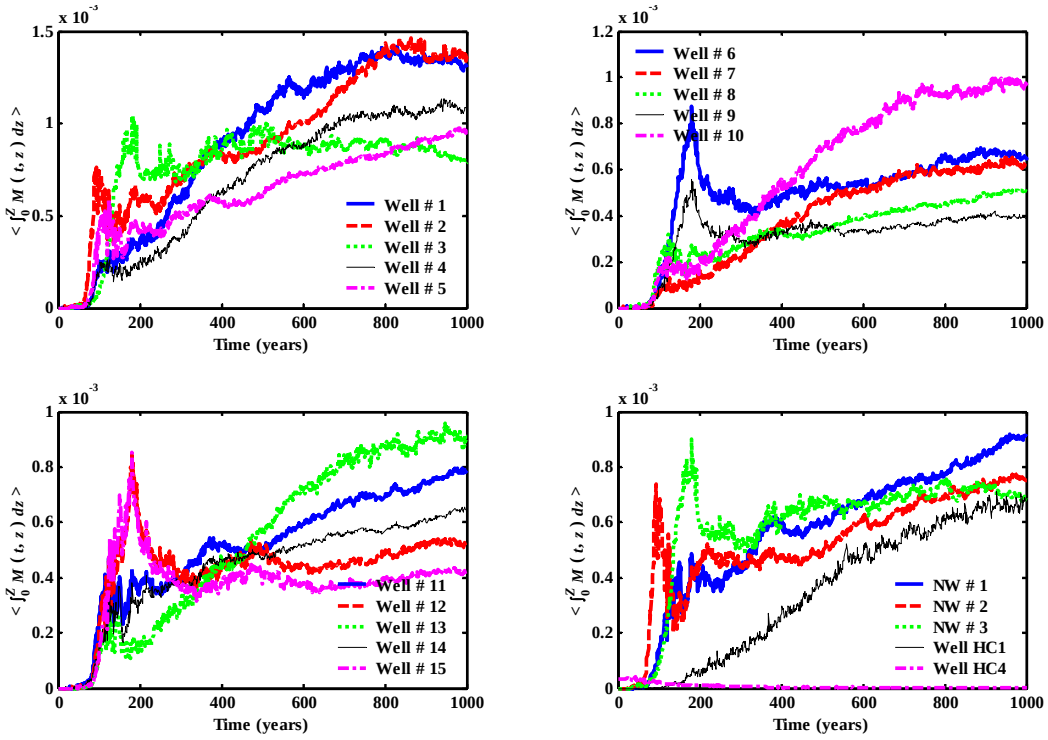

Figure 20. Vertically integrated resident mass in the vicinity of 20 potential well locations.

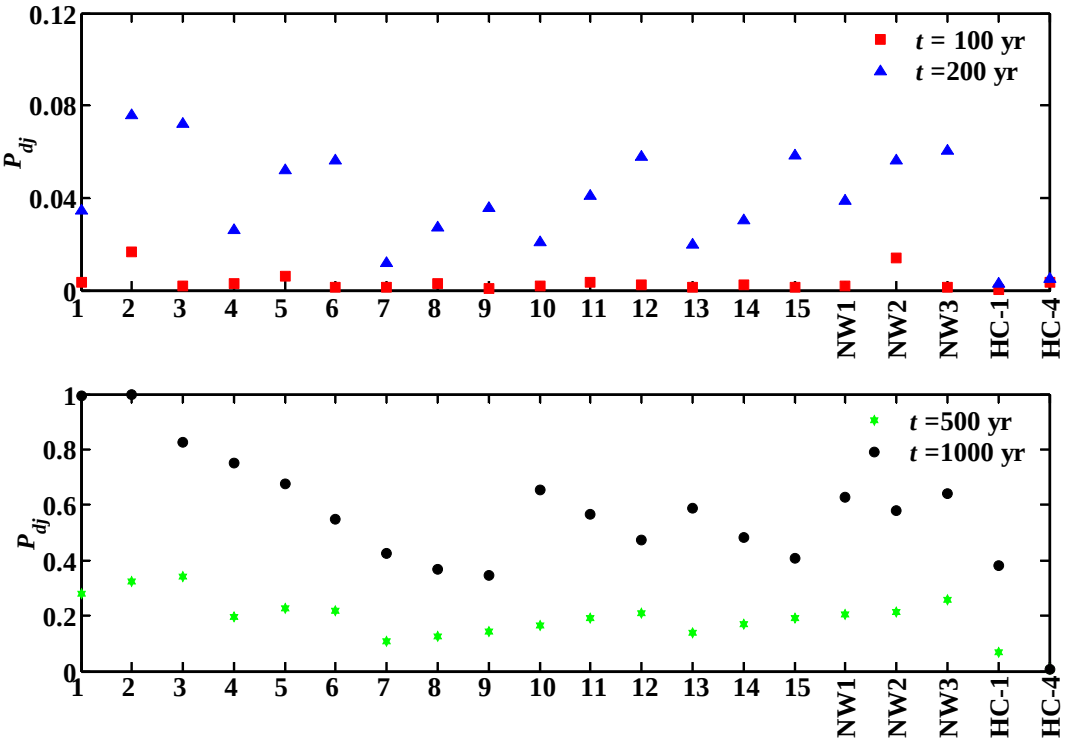

Figure 21. Detection probability for the 20 potential wells at different times.

It is important to mention that because these probabilities are based on the integration of the resident mass, it may attain values above 1.0. This is because particles may reside in the well for more than one time step and thus these particles are counted more than once. When $M_{ji}(t, z)$ is integrated across the z- and t-dimensions, it can yield values for W_{ji} larger than 1.0 in certain realizations. When P_{dj} is computed by averaging W_{ji} over all realizations, it may attain values larger than 1.0. Therefore, the P_{dj} values are normalized relative to the largest value among the 20 potential well locations. This is justified by the fact that the interest here is not in the absolute values of these probabilities, but rather in the relative magnitude of the detection and success probabilities for the different wells and different well combinations.

Figure 21 shows different patterns for the detection probability, P_{dj}, at different times. At 100 years, the central wells on the different CPs attain higher detection probability than the edge wells. However, for t = 200, and 500 years, detection probability increases from the western-edge well to the eastern-edge well. At 1,000 years, the trend is reversed and detection probability decreases from the western-edge well to the eastern-edge well. This can be explained as follows. Two factors affect the results, the time at which detection probability is computed and the velocity encountered by each plume (thus residence time within well vicinity). At 100 years, only few realizations traveled far from the cavity and are located along the mean flow direction thereby hitting the central wells. At intermediate times, fast realizations (mostly to the eastern side of the cavity and the eastern side of the mean plume trajectory) contribute to the eastern-edge wells and lead to the increase in detection probability from west to east. At late times (t = 1,000 years), the slower western realizations arrive to the different CPs and as they are migrating slowly, the particles reside for a long time within the well vicinity, thereby contributing to higher $M(t, z)$, W_{ji}, and P_{dj} at the western-edge wells compared to the eastern-edge wells.

The next step in the analysis is to compute the first probability term on the right-hand side of Equation (6) for each CP. This term expresses the probability that the mass of the radionuclide plume that crossed the CP from time zero to time t relative to the total mass is less than or equal to the parameter α. Therefore, for each time and each CP, the number of realizations satisfying the condition $\left(\frac{1}{M_{total}} \int_0^t Q(\tau; x_k)\, d\tau \le \alpha \right)$ is divided by the total number of realizations to obtain this probability term. Figure 22 displays the values of these probabilities for the five CPs at four times (t = 100, 200, 500, and 1,000 years) and for eight values of the parameter α. As can be seen, the probability decreases as time increases and also as one gets closer to the cavity. For a fixed time and the same CP, when α increases, the probability increases, indicating that more realizations satisfy the condition $\left(\frac{1}{M_{total}} \int_0^t Q(\tau; x_k)\, d\tau \le \alpha \right)$. The results in Figure 22 also indicate that as the distance between the cavity and the CP increases, this probability term increases, but the rate of increase is much higher for late times than for early times. For example, at t = 100 years, the probability term is almost constant for all CPs and all α values, whereas for t = 1,000 years, this probability term changes from a value between 0.5 and 0.6 to a value close to 0.7 as one moves from CP #1 to CP #5.

The last step in this analysis is to compute the success probability for each well according to Equation (6). This success probability is the result of multiplying the probability that α or less

crosses the CP passing through the well by the particular well's detection probability. Since this probability term requires the probability that a mass of α or less crosses the CP passing through the well, it is not computed for wells HC-1, HC-4, NW1, NW2, and NW3, as no control planes are analyzed for these wells. Figures 23 and 24 show the success probability for the potential wells at two values of α (0.01 and 0.04). It is first seen that no significant differences exist between the two values of α except for an increase in the success probability for $\alpha = 0.04$ at 1,000 years. It is also seen that Figures 23 and 24 exhibit patterns similar to those of Figure 21.

Consistent with the previous set of analyses, wells 1, 2, and 3 located at CP #1 have the highest potential for success in detecting the plume. As one moves away from the cavity, success potential decreases as the variability in plume trajectory dictated by the fractured system at Shoal decreases the chance of a well to intercept a large number of the stochastic plumes. However, wells on CPs #4 and #5 exhibit better success probability than wells at CP #3 at 500 and 1,000 years. This is attributed to the interplay between fast-moving realizations and short resident time for particles around different wells and the opposite interplay between slow-moving realizations and longer residence time for particles. Also, the fractured system may cause some of the wells to be always located along a fracture or in a matrix block (based on fracture network and conditioning data). Thus, the success probability exhibits different patterns at different times. This is explained earlier in discussing the patterns of the detection probability P_{dj}, at different times, which dictate the patterns of the success probability, P_s.

From this analysis, it can be concluded that a well located on CP #1 is a good choice. As mentioned earlier, the wells contributing to the long-term monitoring network at Shoal need to be reasonably spaced to meet the monitoring objectives as well as be placed with regard to practical issues such as drill-rig access. Therefore, if a well on CP #1 is selected as part of the monitoring network and it has a high chance of success in detecting the plume migration, other wells can be located on CPs that are farther away from the cavity. It can be seen from Figures 23 and 24 that many of the other wells have generally equivalent success probabilities, with the exception that wells on CP #3 (wells 7, 8, 9) tend to be lower. Therefore, there are a number of other wells that represent good choices to augment a well on CP #1 and form a three-well monitoring network.

3.3 Third Design Tool: Monitoring Efficiency Model (MEMO)

Wilson *et al*. (1992) developed an analytical monitoring efficiency model (MEMO) to assist in the design of monitoring well networks. Their model quantifies the monitoring efficiency of a given monitoring well network by determining the areas within a potential contaminant source area where a release of that contaminant would or would not be detected by the monitoring well network. Monitoring efficiency is defined as the ratio of the area of detection to the total area of the source. For example, a detection efficiency of 90 percent in the Wilson *et al*. (1992) model means that releases occurring over 90 percent of the source area would be detected by the monitoring wells, and releases occurring over the remaining 10 percent of the area would not be detected.

3.3.1 Summary of the MEMO Approach

Wilson *et al*. (1992) determine the monitoring efficiency using a simplified analytical transport model. They start by defining a grid of potential contaminant source points within the potential source area. At each source point, a contaminant plume is generated using an analytical contaminant transport solution. If the plume is intersected by a monitoring well before it migrates beyond a specified boundary, the source point is considered to be detected. After

checking each grid point to determine whether the plume released from that point is detected or not, the monitoring efficiency is calculated. The results are then provided in terms of maps showing the areas from which contaminant releases would not be detected. An illustration of the application of this approach is shown in Figure 25 adapted from Wilson *et al*. (1992).

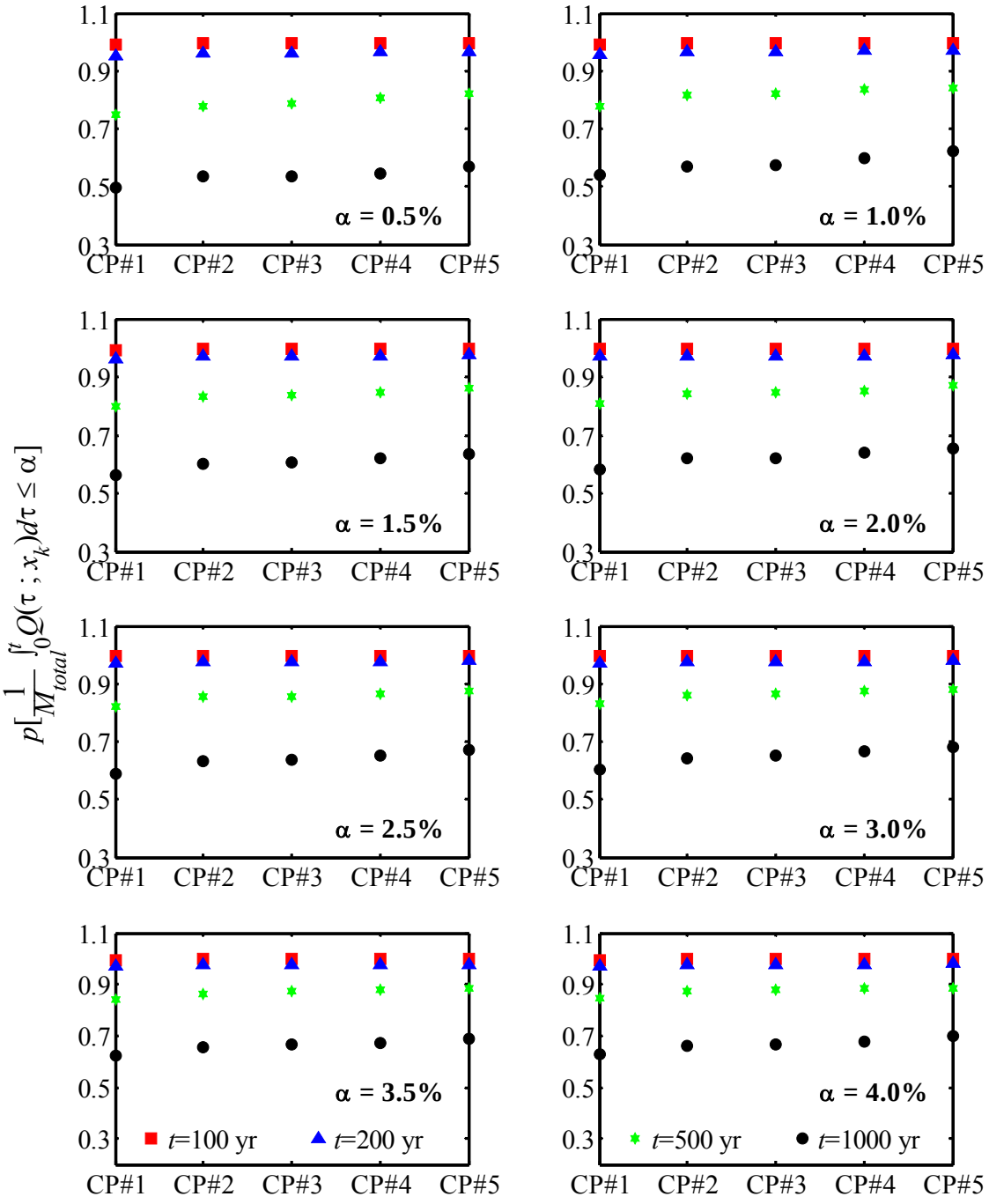

Figure 22. The probability that the mass that crossed the CP from time zero to time t is less than or equal to the percentage α.

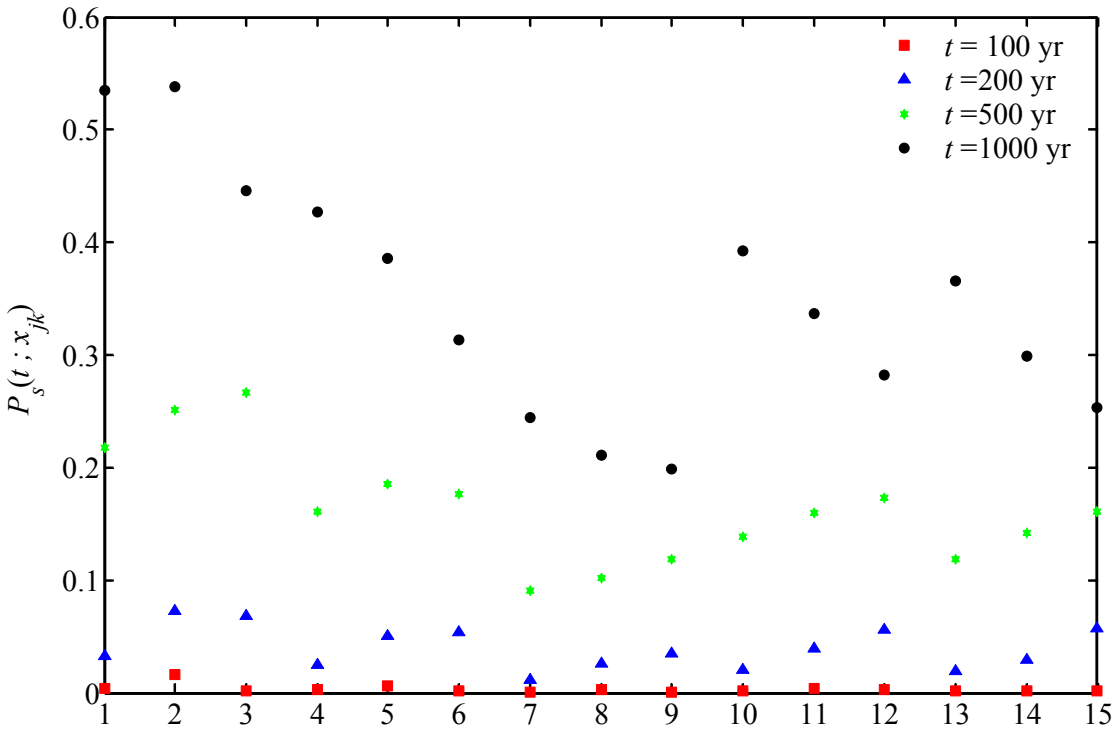

Figure 23. Success probability of individual wells at different times for α = 1 percent.

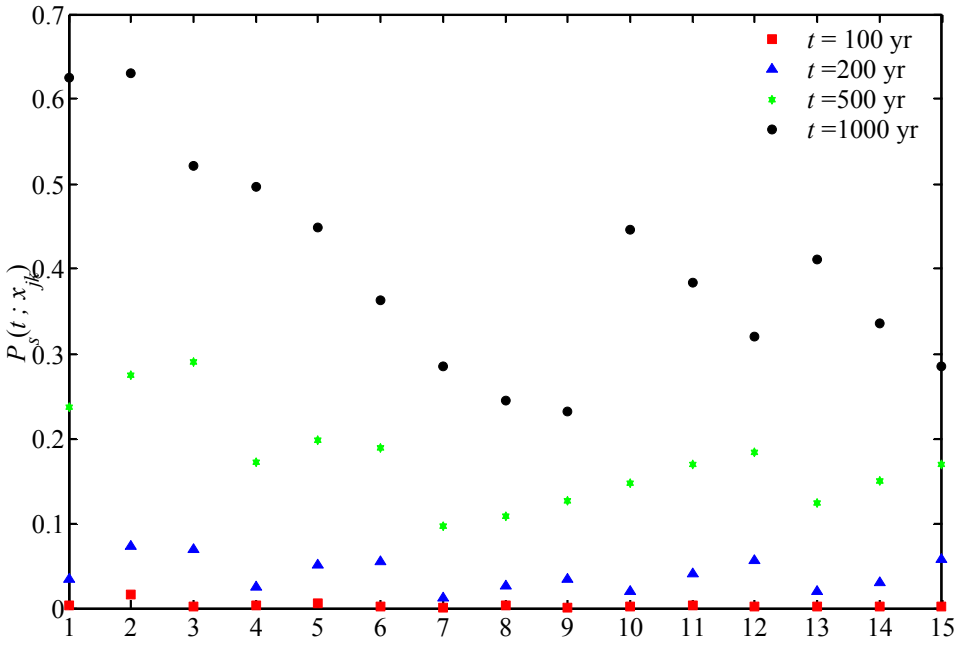

Figure 24. Success probability of individual wells at different times for α = 4 percent.

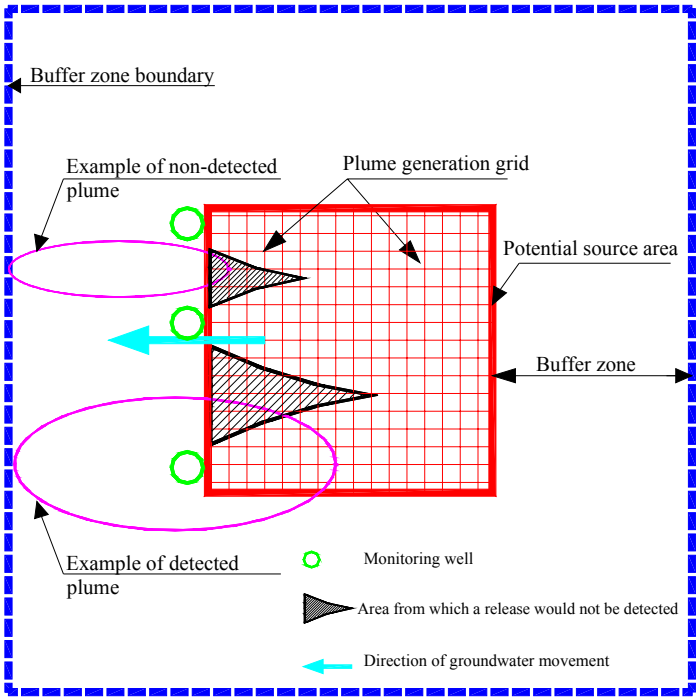

Figure 25. Schematic diagram showing the application of the MEMO model (adapted and modified from Wilson *et al.*, 1992).

The critical geometric elements in this approach are the potential source area, the grid of potential source points, the buffer zone boundary, and monitoring well locations. The buffer zone boundary is defined as the limit to which a plume can migrate before it should be detected, and serves as the plume migration limit for early warning detection of a contaminant release (Wilson *et al*., 1992). If a plume moves beyond this limit without being detected by one of the monitoring wells, it is considered to be undetected. Figure 25 shows examples of detected and nondetected plumes and two distinct regions defined by source grid points from which generated plumes were not detected by monitoring wells prior to passing the buffer zone boundary. According to Wilson *et al*. (1992), general criteria for establishing buffer zone widths include distance to property boundaries and neighboring dwellings, distances to groundwater supply wells or surface water bodies, the velocity of groundwater movement, and the relative costs and benefits of providing early detection of a contaminant release.

Although the Wilson *et al*. (1992) approach was mainly applied for deterministic groundwater contamination problems, the authors indicate that the sensitivity of the monitoring efficiency estimate to variations in groundwater flow direction should be considered, particularly when no field data are available. Therefore, in adapting this approach for estimating the efficiency of the proposed monitoring well network at Shoal, the uncertainty in the flow and transport parameters should be accounted for in the analysis.

3.3.2 Application of MEMO to Shoal

To adapt this approach and apply to Shoal, some modifications are necessary. Wilson *et al.'s* approach relies on simplistic transport solutions that assume deterministic homogeneous conditions and thus can be obtained analytically. For Shoal's model and to apply this approach, the particle plume resulting from each stochastic realization is represented by the trajectory of the plume's center of mass (c.o.m.). The critical geometric elements in this approach are adapted and changed as follows. The potential source area and its location are known with certainty at Shoal. The grid of potential source points is not applicable in this case as the migration at Shoal is occurring from the cavity toward the downgradient direction. The variability induced in Wilson *et al.'s* approach by releasing the plume from the different potential source points is replaced for Shoal by the variability in the plume trajectory from one realization to another. The buffer zone boundary is replaced by the compliance boundary at Shoal (assumed to be the MCL-based contaminant boundary), where a plume is considered to be detected by a well if its c.o.m. passes in the vicinity of that well before reaching the compliance boundary.

To simplify the analysis, a rectangular detection zone is determined for any set of wells to be evaluated. The sides of this rectangle are specified by subtracting half a grid cell ($0.5\ \Delta x$) from the smallest x'-coordinate among the wells and adding $0.5\ \Delta x$ to the largest x'-coordinate and doing the same in the y'-direction. Then, a plume is considered to be detected if its c.o.m. trajectory passes inside this detection zone before reaching the buffer zone boundary or the compliance boundary. The efficiency of the network (any set of wells) is obtained by dividing the number of realizations where plume is detected by the total number of realizations.

It is of interest to evaluate the differences between two configurations of the potential wells. The first configuration consists of the potential wells 1 through 15 in addition to HC-1, whereas the second configuration consists of the 15 potential wells only. The rectangular detection zone for each configuration is determined as discussed above and the detection efficiency is computed for each configuration. Figure 26 displays the potential well locations for the first configuration, the domain boundary, the detection zone, the cavity location, and the c.o.m. trajectory for the detected plumes, whereas Figure 27 displays the results for the nondetected plumes for the same configuration. The number of detected realizations for this configuration is 162 out of 1,000 realizations. This gives a detection efficiency for this configuration of 16.2 percent (162 detected plumes out of 1,000). It is important, however, to note that many of the nondetected plumes are essentially slow-moving plumes that do not even approach the detection zone during the 1,000-year simulation time. Therefore, this detection efficiency should be adjusted by dividing by the number of moving realizations instead of the total number of realizations. This number is determined by counting the realizations for which the c.o.m. trajectory crossed the boundary of the detection box that is close to the cavity (i.e., trajectories that satisfy the condition that $\text{Max}\ (y'_{\text{c.o.m}}) \geq \text{Min}\ (y'_{\text{detection box}})$). This number is found to be 177. Thus, the adjusted efficiency for this first configuration is about 91.5 percent (162 detected plumes out of 177 moving plumes).

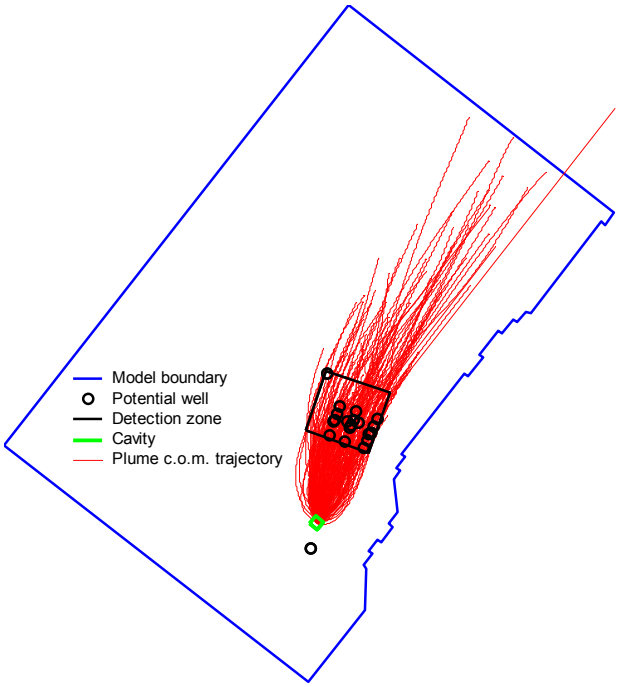

Figure 26. Trajectories of detected plumes superimposed on the potential well locations for the first configuration, where well HC-1 is included. Rectangular detection zone and the test cavity are also shown.

Figure 27. Trajectories of nondetected plumes superimposed on the potential well locations for the first configuration, where well HC-1 is included. Rectangular detection zone and the test cavity are also shown.

Figures 28 and 29 display the results for the second configuration, which does not include well HC-1 in the analysis. The unadjusted detection efficiency for this configuration is about 13.1 percent and the adjusted efficiency is about 74 percent (131 detected plumes out of 177 moving plumes). The removal of HC-1 leads to a smaller detection box, especially from the western side, which causes about 30 plume trajectories to pass by the western edge of the smaller detection zone without being detected. Although well HC-1 seems to enhance the overall efficiency of the entire network composed of all potential wells, being outside the compliance boundary and its own very small detection probability (see Figure 21) minimize the benefit of including it in the long-term monitoring network of the site (from a detection efficiency standpoint).

Individual wells are also analyzed for detection efficiency. In this case, a criterion is set such that a plume is considered detected by a well if the vertically integrated resident mass within the well vicinity attains a percentage mass of value α (e.g., 1 percent or 2 percent) when or before an equivalent percentage reaches the compliance boundary. The number of detections is then determined. The results of this analysis are shown in Figure 30. One would expect the number of detections for a certain well to increase as α increases because larger values of α require more time to cross the compliance boundary, thus providing more chance for the well to detect the plume. However, the results in Figure 30 display the opposite trend of decreasing numbers of detection with increasing α. This is attributed to the criterion that the plume is detected if and only if a total percentage mass of value α or more reside within the well vicinity before an equivalent cumulative percentage α crosses the compliance boundary. In this case, when α increases, the plume may cross the compliance boundary before meeting the detection criterion, which becomes more difficult to meet for larger values of α. Figure 30 also shows that in general, eastern wells have larger numbers of detections than western wells (e.g., wells 5 and 6 have larger numbers of detections than well 4, and wells 8 and 9 have larger numbers than well 7). This is again attributed to the faster plumes that migrate to the eastern side of the cavity, which enables the eastern wells to detect a certain mass percentage α before an equivalent mass crossed the compliance boundary.

Finally, multiple networks, three wells each, are formed and analyzed for detection efficiency. The wells comprising each network are listed in Table 6. A total of 76 networks are analyzed and their detection efficiencies are computed in a manner similar to the analysis of the two configurations presented in Figures 26 through 29. It is important to recognize that for networks of multiple wells, the plume is considered detected if its trajectory passes through the rectangular detection zone encompassing the wells. This is different than individual well analysis presented above.

Well HC-1 is one of the three wells in 12 of the networks. Including HC-1 leads to a larger detection box, encompassing more plumes on the western side, and thus higher network efficiency. Although HC-1 seems to enhance the overall efficiency in the MEMO analysis, its actual effect would be much diminished because the majority of modeled plumes are at depths much greater than the well by the time they have traversed the distance from the cavity to HC-1 (Figure 31), and because the well spacing in that larger box is unlikely to intercept all the plumes passing through it (compare Figures 26 and 27 with Figures 28 and 29). Again, the location of HC-1 outside the compliance boundary and its own very small detection probability (see Figure 21) minimize the benefit of including it in the long-term monitoring network, at least at the expense of another well location.

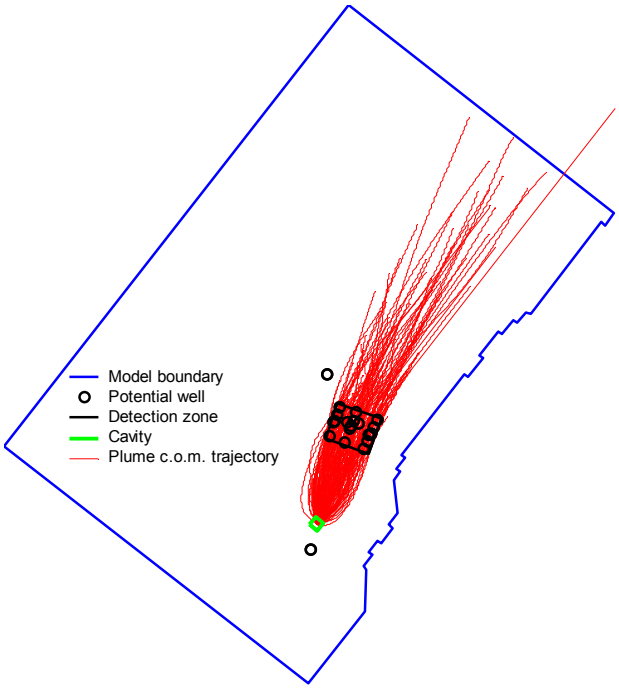

Figure 28. Trajectories of detected plumes superimposed on the potential well locations for the second configuration, where well HC-1 is excluded. Rectangular detection zone and the test cavity are also shown.

Figure 29. Trajectories of nondetected plumes superimposed on the potential well locations for the second configuration, where well HC-1 is excluded. Rectangular detection zone and the test cavity are also shown.

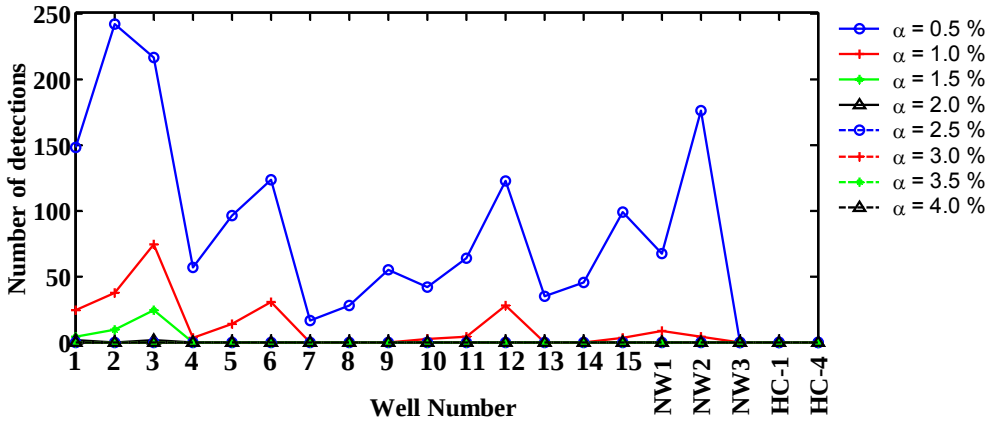

Figure 30. Number of detections by individual wells where the criterion that the resident mass within the well vicinity reaches a value of α before an equivalent mass crosses the MCL-based boundary is employed.

Table 6. Well assignments in the evaluated monitoring networks.

Network #	First Well	Second Well	Third Well	Network #	First Well	Second Well	Third Well
1	1	4	5	39	4	7	9
2	1	5	6	40	5	7	8
3	1	4	6	41	5	8	9
4	2	4	5	42	5	7	9
5	2	5	6	43	6	7	8
6	2	4	6	44	6	8	9
7	3	4	5	45	6	7	9
8	3	5	6	46	4	10	11
9	3	4	6	47	4	11	12
10	1	7	8	48	4	10	12
11	1	8	9	49	5	10	11
12	1	7	9	50	5	11	12
13	2	7	8	51	5	10	12
14	2	8	9	52	6	10	11
15	2	7	9	53	6	11	12
16	3	7	8	54	6	10	12
17	3	8	9	55	4	13	14
18	3	7	9	56	4	14	15
19	1	10	11	57	4	13	15
20	1	11	12	58	5	13	14
21	1	10	12	59	5	14	15
22	2	10	11	60	5	13	15
23	2	11	12	61	6	13	14
24	2	10	12	62	6	14	15
25	3	10	11	63	6	13	15
26	3	11	12	64	1	HC-1	11
27	3	10	12	65	1	HC-1	12
28	1	13	14	66	2	HC-1	11
29	1	14	15	67	2	HC-1	12
30	1	13	15	68	3	HC-1	11
31	2	13	14	69	3	HC-1	12
32	2	14	15	70	4	HC-1	11
33	2	13	15	71	4	HC-1	12
34	3	13	14	72	5	HC-1	11
35	3	14	15	73	5	HC-1	12
36	3	13	15	74	6	HC-1	11
37	4	7	8	75	6	HC-1	12
38	4	8	9	76	NW1	NW2	NW3

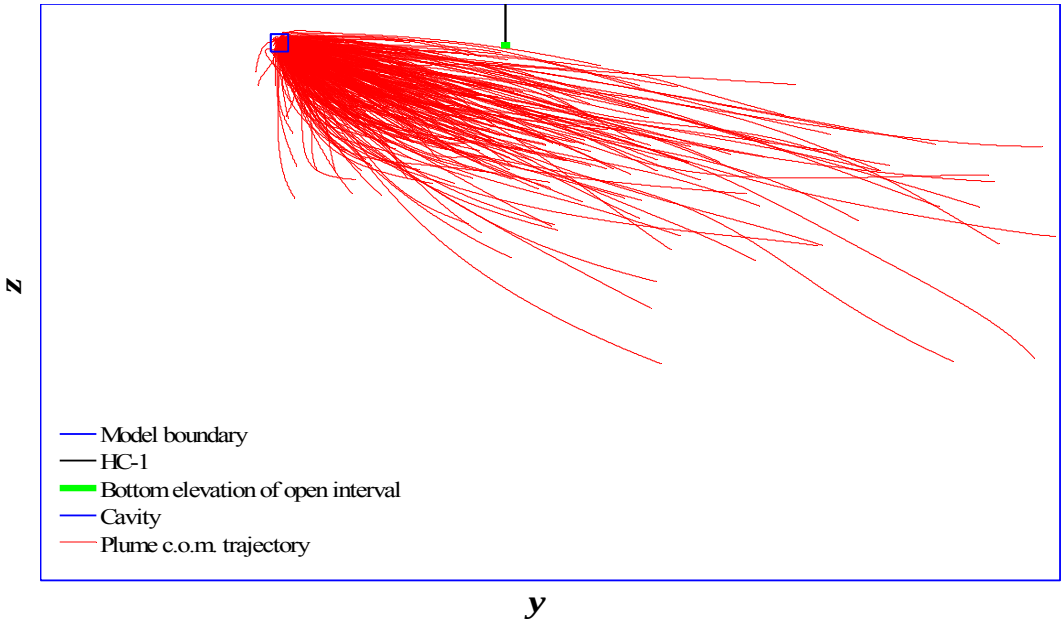

Figure 31. Vertical section through the model domain showing plume trajectories passing below the elevation of the open interval in well HC-1. Note that many of the plumes are also not coincident with the *x*-*y* location of the well.

The detection efficiency for these 76 networks is shown in Figure 32. The figure reveals a number of interesting results. The first network composed of wells 1, 4, and 5 has a low detection efficiency of about 40 percent, whereas network 2, composed of wells 1, 5, and 6, has a higher efficiency of about 70 percent. Similarly, networks 36 and 37 exhibit the same pattern. To explain these findings, Figure 33a shows a plot of the well locations and detection zones relative to the plume trajectories (only a small number of trajectories is plotted for clarity) for networks 1 and 2 (superimposed); plotted in Figure 33b are the detection zones for networks 36 and 37. A larger number of trajectories pass outside the right edge of the detection zone in network 1, whereas the larger detection zone of network 2 captures these trajectories. The same is true for the comparison between networks 36 and 37. Similar comparisons are shown in Figures 34 and 35, where networks 39 and 40 are compared, 64 and 65 are compared, and 69 and 70 are compared. In each case, one detection box is much larger than the other resulting in higher detection efficiency.

It can also be seen from Figure 32 that the network composed of wells NW1, NW2, and NW3 has a low detection efficiency compared to other networks. This is attributed to the fact that these three wells are close to each other and the detection box enclosing them is small compared to other networks, which leads to a smaller number of trajectories crossing this small box. It is also clear that many of the networks that include well HC-1 have better detection efficiency than most of the tested networks. This is because of the location of HC-1, which allows the detection box to be very large, leading to this high detection efficiency. However, as mentioned earlier, well HC-1 has a very low detection probability as shown in Figure 21 and is located outside the compliance boundary and thus is not a good choice for the long-term monitoring network from the detection efficiency perspective.

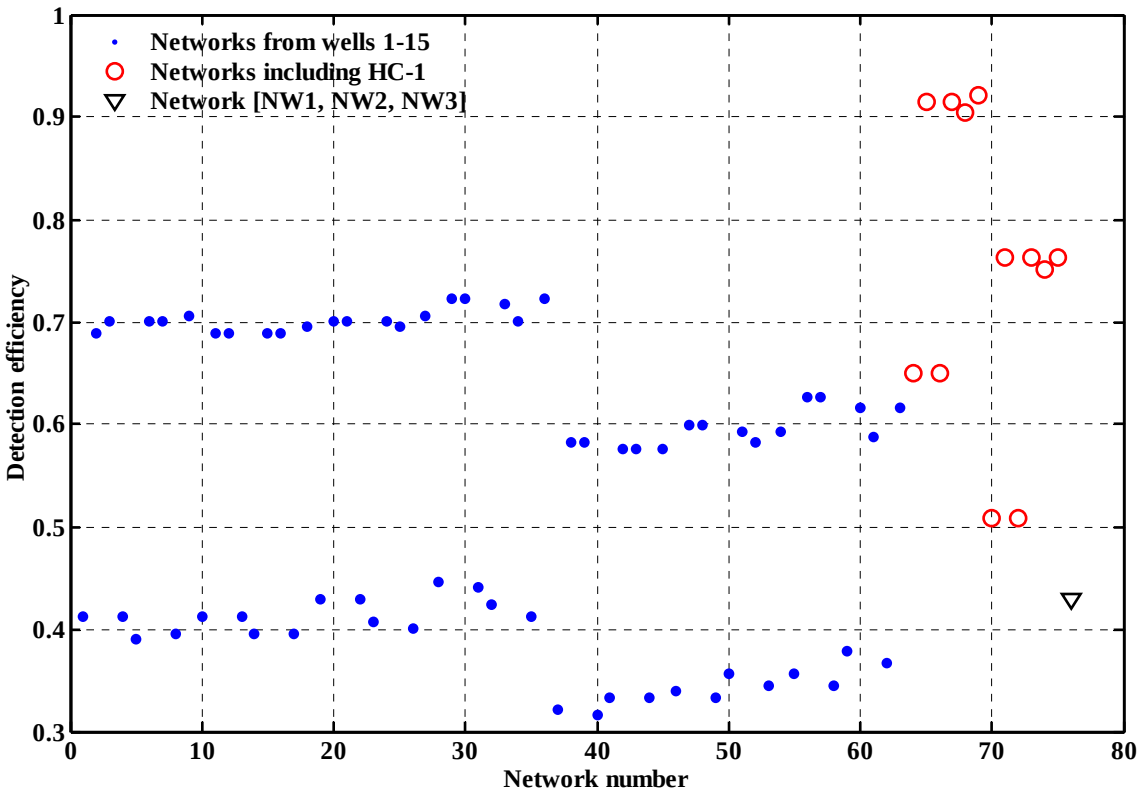

Figure 32. Detection efficiency for 76 three-well networks as computed by geometric considerations where a network detects a plume when its trajectory passes within the network's rectangular detection zone.

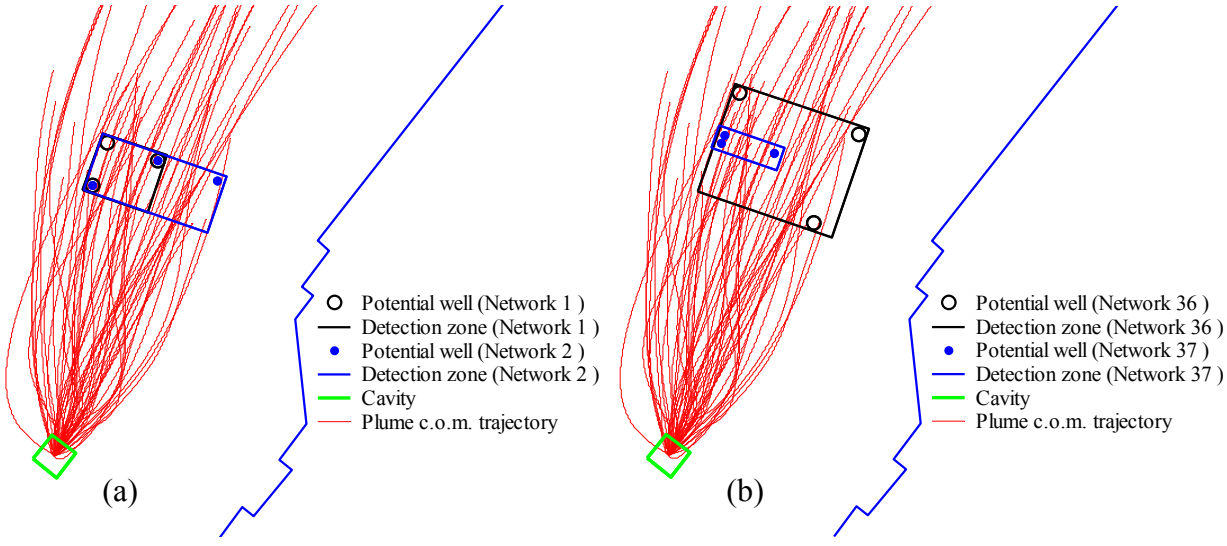

Figure 33. Detection zones for networks 1 and 2 (a) and 36 and 37 (b).

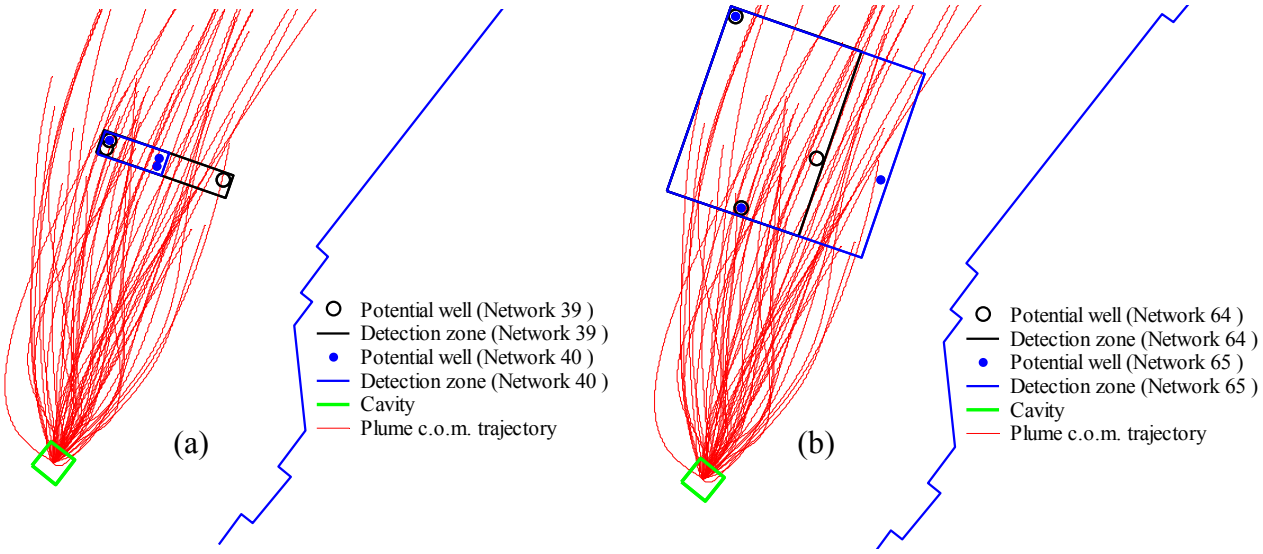

Figure 34. Detection zones for networks 39 and 40 (a) and 64 and 65 (b).

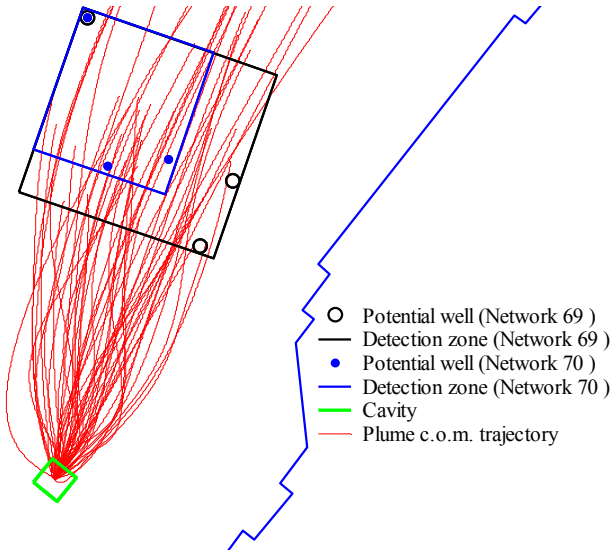

Figure 35. Detection zones for networks 69 and 70.

Figure 32 shows four bands of networks with similar efficiencies (neglecting the networks that include HC-1). Twenty well combinations achieve detection efficiencies around 70 percent. Of these, networks 29, 30, 33, and 36 attain the highest efficiency. Each of these includes one well on CP #1 and two on CP #5, such that two network wells would monitor the compliance boundary but not provide as much reaction time as wells on other CPs in the event of contaminant detection.

Selection of the optimum monitoring network combines the findings of the three design tools. First, only networks comprised of three new wells, as compared to HC-1, are considered. This is further limited to networks in the highest tier of detection efficiency, as

computed using the third tool, MEMO. Preference is then given to networks with wells that provide the 50-yr reaction time (part of the analysis of the first tool). Finally, selection among the essentially equivalent networks remaining is based on the results of the individual well performance measures given by the second tool. The best individual well performance was attained by well 2. It is on the first CP (best performing in the first tool) and also on the mean trajectory of the center of mass. The high efficiency networks including well 2 that also meet the other criteria are networks 6, 15, and 24. Network 6 is selected as the optimum due to the poorer performance of wells 7 and 9 (and CP #3 in general) in network 15, and the possible absence of reaction time for wells 10 and 12, depending on plume trajectory, of network 24. Network 6 is comprised of wells 2, 4, and 6.

Figure 36 shows the locations of the proposed three-well network relative to the test cavity and the computed MCL-based boundary (Pohll and Pohlmann, 2004). The proposed three wells are reasonably located relative to the cavity at least from a qualitative inspection of Figure 36. Once again, these locations may be slightly modified to avoid any practical limitations or problems and to maximize the benefit from these wells in validating the model. In addition to the proposed new wells, existing wells HC-1 and HC-4 are proposed for inclusion in the network. Neither had good individual well performance, but they are low-cost additions that will provide additional areal coverage.

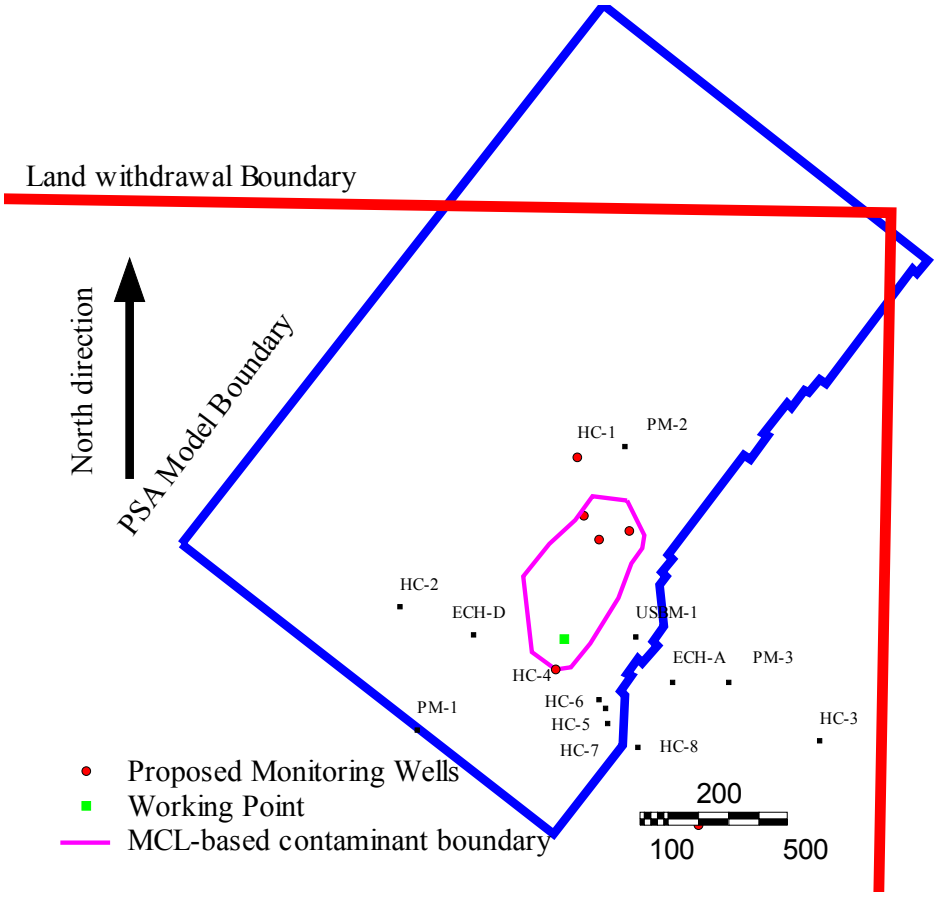

Figure 36. Proposed long-term monitoring network (three new wells and two existing wells) relative to the test cavity and the computed MCL-based contaminant boundary.

3.4 Completion Interval

Having determined the three new well locations to be used for detection monitoring and validation purposes, the first tool (Hudak, 1994) can be used to provide some guidance into the completion or sampling interval for each well. Similar to the analysis performed using the plume width and the x'-location of the plume center of mass for the purpose of determining the minimum number of wells, N_i, needed to span a siting horizon, the plume height and the z-location of the center of mass are analyzed to obtain N_i in the vertical direction. To first obtain the maximum interval spacing, S_i, the simulation results for the five CPs where the plume height at each CP is reported for each realization of the stochastic flow and transport model at Shoal are analyzed. To summarize the results for the different times, different CPs, and different realizations, Table 7 shows the prediction quantiles (PQ) obtained from the 1,000 realizations of plume heights. These are obtained in a similar manner to the analysis reported earlier in Section 3.1.3. The results for the plume height analysis are summarized in Table 7. It can be seen that on average, the plume height slightly exceeded 400 m at 1,000 years. At 100 years, however, the plume height is about 125 m on average. For each CP and for each time considered, the parameter S_i is obtained as the 50 percent PQ of the plume height as it crosses the CPs.

Table 7. Prediction quantiles (PQ) for the plume height at different times and for the five CPs.

Plume height when crossing the CP (m)												
Control	t = 100 years			t = 200 years			t = 500 years			t = 1,000 years		
Plane	2.5% PQ	50% PQ	97.5% PQ	2.5% PQ	50% PQ	97.5% PQ	2.5% PQ	50% PQ	97.5% PQ	2.5% PQ	50% PQ	97.5% PQ
CP #1	5.4	120.2	444.5	13.9	185.1	631.3	38.0	287.1	979.9	46.9	401.4	1102.0
CP #2	5.2	137.3	396.4	9.0	169.6	552.5	27.3	282.3	953.7	34.6	404.0	1095.4
CP #3	13.1	123.7	475.9	3.8	158.3	594.5	22.2	278.6	962.1	40.4	403.9	1100.3
CP #4	25.2	123.5	545.4	9.3	161.5	568.6	22.9	280.9	935.4	41.8	403.3	1097.1
CP #5	9.1	100.5	489.5	13.5	174.5	532.4	21.6	280.2	866.3	36.3	404.3	1049.4

For each CP and at each time considered, the zone of potential contaminant migration, W_i, in the vertical direction is obtained by analyzing the distribution of the z-coordinate of the plume center of mass as it crosses the CPs. Table 8 displays the PQs for the z-position of the center of mass of the plume. To obtain the parameter W_i, the difference between the 97.5 percent PQ (representing the upper bound or the uppermost plume) and the 2.5 percent PQ (representing the lower bound or the lowermost plume) is computed and taken as a representation of the zone of potential migration in the vertical direction.

Table 8. Prediction quantiles (PQ) for the z-position of the plume center of mass at different times and for the five CPs.

Vertical coordinate z of the plume center of mass when crossing the CP (m)												
Control	t = 100 years			t = 200 years			t = 500 years			t = 1,000 years		
Plane	2.5% PQ	50% PQ	97.5% PQ	2.5% PQ	50% PQ	97.5% PQ	2.5% PQ	50% PQ	97.5% PQ	2.5% PQ	50% PQ	97.5% PQ
CP #1	924.1	1157.2	1226.9	841.8	1121.2	1227.7	844.8	1090	1218	806.7	1077	1211.3
CP #2	918.1	1153.9	1219.1	875	1116.7	1224.2	799.2	1074.8	1215	773.9	1059.9	1211
CP #3	831.9	1156.1	1215.9	863.9	1117.5	1228.2	776.6	1074.3	1214.9	779.8	1057.5	1210
CP #4	698.6	1133.5	1217.3	854	1111.9	1221	779.4	1068.7	1216.5	751.8	1047.9	1212.5
CP #5	692.7	1136.9	1219.9	798.8	1102.9	1221.1	758.7	1057.5	1213.6	738.7	1036.5	1208.6

After determining the two parameters S_i and W_i for all CPs, Equation (1) is used to obtain the minimum number of sampling intervals needed for well 2 (at CP #1) and wells 4

and 6 (at CP #2). Table 9 shows the values of S_i, W_i, S_i/W_i, and N_i for each CP and all times considered. It can be seen from Table 9 that the required number of sampling intervals in the vertical direction is generally between one and two for CPs #1 and 2. Based on these results, it is reasonable to assume that one interval for each well will have a good chance of detecting the plume migration if it reaches to that particular CP.

Table 9. Parameters of Equation (1) and the minimum number of intervals, N_i, to span each CP (or well) at different times.

S_i, W_i, siting horizon efficiency (S_i / W_i), and N_i for the five CPs and the different times																
Control	t = 100 years				t = 200 years				t = 500 years				t = 1,000 years			
Plane	S_i	W_i	S_i/W_i	N_i	S_i	W_i	S_i/W_i	N_i	S_i	W_i	S_i/W_i	N_i	S_i	W_i	S_i/W_i	N_i
CP #1	120.2	302.8	0.40	2	185.1	385.9	0.48	2	287.1	373.2	0.77	1	401.4	404.6	0.99	1
CP #2	137.3	301.0	0.46	2	169.6	349.2	0.49	2	282.3	415.8	0.68	1	404.0	437.1	0.92	1
CP #3	123.7	384.0	0.32	3	158.3	364.3	0.43	2	278.6	438.3	0.64	1	403.9	430.2	0.94	1
CP #4	123.5	518.7	0.24	4	161.5	367.0	0.44	2	280.9	437.1	0.64	1	403.3	460.7	0.88	1
CP #5	100.5	527.2	0.19	5	174.5	422.3	0.41	2	280.2	454.9	0.62	1	404.3	469.9	0.86	1

The above analysis indicates that one sampling interval per well should be sufficient for detection monitoring. However, the analysis does not provide guidance on where to place this sampling interval for each well. The other tools discussed in Section 3 provide some guidance in this regard. By integrating the resident mass for each well in the time domain, one obtains a vertical profile for mass distribution in each well's vicinity, which provides some guidance on the selection of the sampling interval location. Figure 37 displays the temporally integrated resident mass (averaged over all realizations) in the vicinity of the 15 potential well locations. Again the vicinity of the wells is defined by the grid cell ($\Delta x \times \Delta y$) where the well is located. It can be seen that for well 2, a high value of resident mass exists at an elevation of about 1,150 m. For well 4, the peak value is at approximately 1,100 m, and for well 6, the high value of the resident mass exists at an elevation of about 1,175 m.

Given this guidance, 15 intervals at different elevations are tested for each well with the interval being 50 m long. The elevations of these intervals for each well are shown in Figure 38. Then, a detection zone of size ($[50 + \Delta z] \times \Delta x \times \Delta y$) centered on the interval center is used to determine the number of plume trajectories that pass through it (i.e., detected by this sampling interval). The number of detections obtained for each interval at each of the three wells is shown in Figure 38. The interval with maximum detection efficiency is shown in red in this figure. It should be remembered that these trajectories are the plume center of mass trajectories and thus plumes that are wide can be detected by the different intervals even if the center of mass trajectory does not cross the detecting zone of these intervals. In other words, the different wells can detect portions of dispersed plumes where the plume center of mass trajectory does not cross the grid cells where these wells are located.

To confirm that the selected intervals are reasonable, Figure 39 plots the plume trajectories in the y-z plane and superimposes the wells and the sampling intervals for wells 2, 4, and 6. The interval for well 2 spanning the elevations 1,065 and 1,115 m, for well 4 spanning the elevations 1,000 and 1,050 m, and for well 6 spanning the elevations between 1,105 m and 1,155 m captures many of the trajectories shown in Figure 39. Based on Figure 37, these intervals are close to the peak of the resident mass in the vicinity of each of the three wells, indicating that these intervals would have a high chance of detecting contaminant mass if plumes arrive close to the wells.

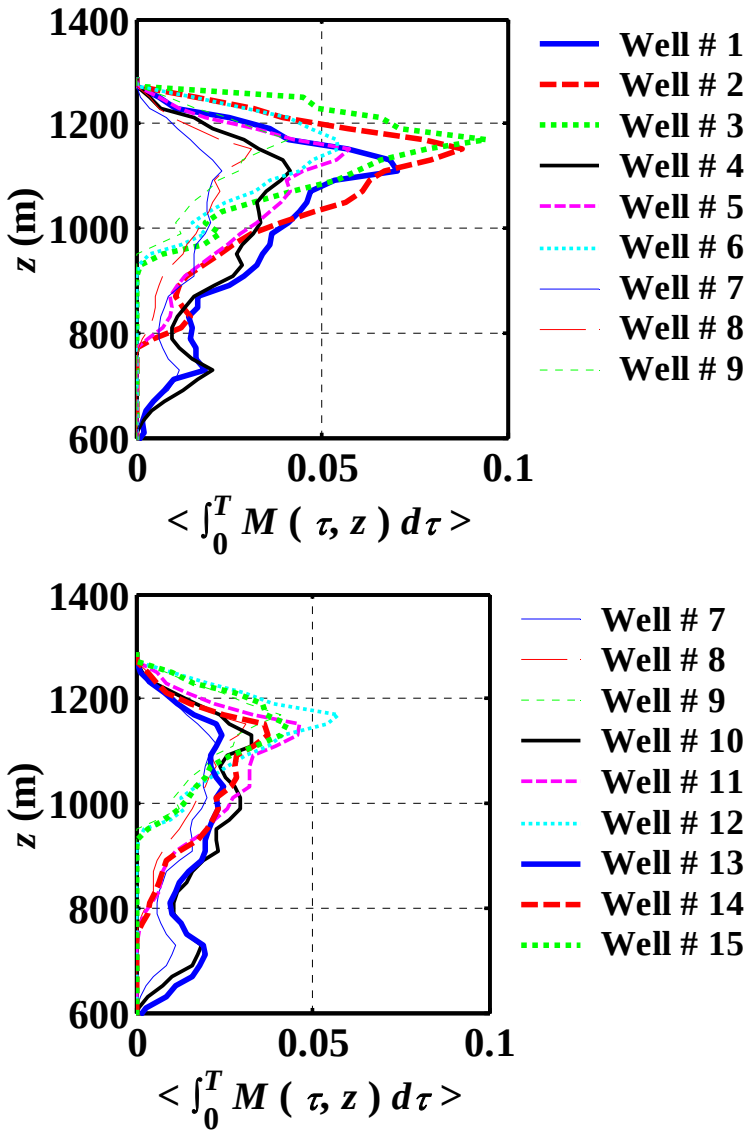

Figure 37. Temporally integrated resident mass in the vicinity of the 30 potential well locations as a function of elevation, *z*.

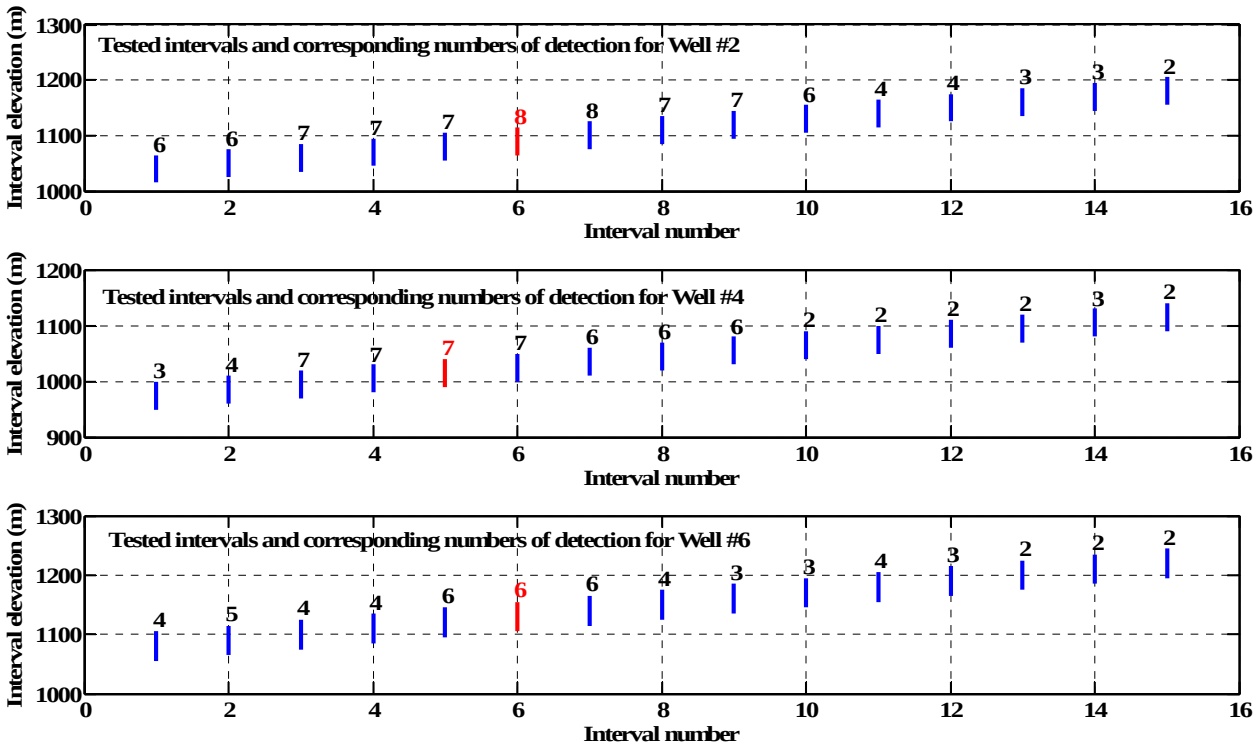

Figure 38. Tested intervals and numbers of detected plume trajectories for each interval for wells 2, 4, and 6.

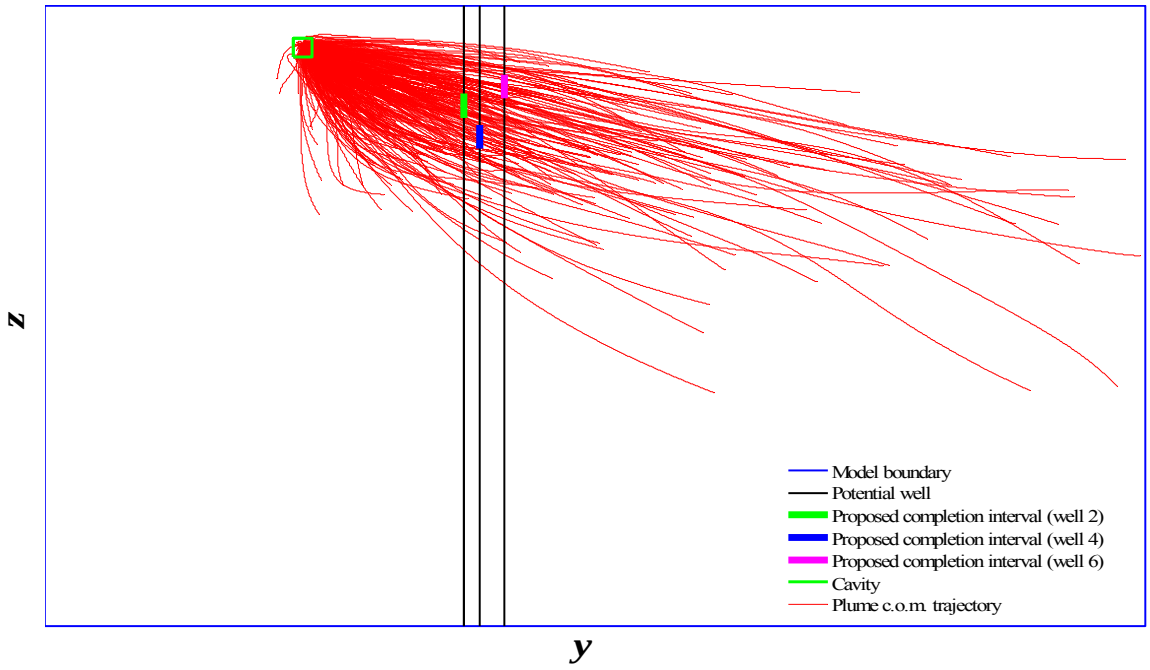

Figure 39. Trajectories of plumes superimposed on the potential well locations. Proposed sampling intervals for wells 2, 4, and 6 are shown.

3.5 Sampling Frequency

Long-term monitoring well networks designed to provide surveillance for contaminated groundwater sites must be sampled at appropriate intervals to ensure timely detection of contaminant migration without being overly conservative. A large sampling interval could miss the contaminant plume and too short a sampling interval could waste millions of dollars (van Dernoot and Williams, 1998). As discussed by Hudak (2001), the U.S. Environmental Protection Agency (EPA, 1994) under stipulations of the Resource Conservation and Recovery Act, requires at least semi-annual sampling for detection monitoring programs. Similar guidelines have been published by state agencies and they differ from state to state. But these agencies may allow for larger sampling intervals if the site owner/operator submits a successful counter proposal (for example, based on low groundwater velocity).

Hudak (2001) devised a simple approach to detection monitoring that considers temporal sampling intervals and evaluated the effects of groundwater velocity on sampling intervals. He concluded that groundwater velocity exerts a strong control on the maximum sampling interval of contaminant detection networks in aquifers. He recommended that one should consider groundwater velocity when defining a detection well sampling interval rather than rely upon a default interval supplied by a regulatory agency.

At Shoal, this simplified approach can be applied to provide some guidance into how frequent the long-term monitoring wells should be sampled. However, the groundwater velocity at Shoal is so small that resulting sampling intervals will likely be very large. For completeness and the possibility of its application to determine sampling frequency at Shoal, Hudak's (2001) approach is briefly described here.

The ability of an n-well monitoring network sampled at interval i to intercept a contaminant plume can be evaluated using the following steps: 1) determine the time t for a contaminant plume originating from the contamination source to reach the buffer zone boundary, 2) recalculate the plume migration distance for a time period $t - i$, 3) position a hypothetical inner buffer zone boundary at the front tip of the shorter, recalculated plume, and 4) calculate the monitoring network's detection efficiency using the inner buffer zone boundary. If the detection efficiency calculated in step 4 is less than the target efficiency, then a) retain the current n-well network, decrease the sampling interval, and repeat steps 1 through 4, or b) retain the current sampling interval, derive a new network with $n + 1$ wells, and repeat step 4. Otherwise, if the detection efficiency in step 4 is above the target, increase the sampling interval and repeat steps 2 through 4. The above procedure continues until the detection efficiency meets the target.

Another approach that can be applied to Shoal is developed by Gibbons (1990), but it requires a set of historical background data and is only beneficial in case some of the radionuclides produced by the test occur naturally in the subsurface. In this case, one would want to distinguish between natural variability of a certain element and variability caused by the nuclear test. As discussed by Gibbons (1990), comparisons typically are made between a set of historical upgradient background measurements and an individual new monitoring measurement, separately in each of a series of downgradient wells. When a single comparison results in statistical significance at the 5 percent level, it is considered as evidence that the disposal facility is impacting groundwater quality, regardless of the number of comparisons made. Another issue is that several commonly used performance indicators have non-normal

distributions that are often resistant to simple data transformation. In addition, a proportion of the observations of these indicator variables is often measured below an established method detection limit. For example, for volatile organic priority pollutant compounds, which are commonly used indicators of contamination, the proportion of nondetected values is often in excess of 95 percent, ruling out the application of traditional statistical methods (Gibbons, 1990).

In an attempt to address these issues, Gibbons (1990) presented a derivation for nonparametric prediction limits for detection monitoring at waste disposal facilities. Specifically, he provided expressions to obtain the probability that at least one of *m* future measurements in each of *k* monitoring wells would not exceed the maximum of *n* previous background or historical samples. To construct the nonparametric prediction limits, Gibbons (1990) began by assuming that the *n* background measurements, presumably upgradient of the contamination source, are drawn from a continuous distribution, but the exact form of that distribution does not need to be known. The next round of sampling is assumed to result in *mk* measurements, presumably from *k* downgradient wells, and in the absence of impacts from the contaminant source, these measurements are assumed to be drawn from the same population or probability distribution of groundwater quality as the background measurements.

For each one of the *k* downgradient wells, there is the possibility of up to $m - 1$ resamples, where *m* is the total number of samples including the original, to rule out laboratory errors and other sources of errors that may lead to a false positive. This means that resampling continues until either a resample results in an indicator value less the maximum of the *n* background samples, or that the total number of samples is *m*. In the latter case, all *m* samples yield values higher than the maximum of the background samples, and the result of the comparison is deemed significant (e.g., the contaminant source impacted the groundwater quality). In this context, Gibbons (1990) defined the γ percent upper prediction limit (for example, the 95 percent upper prediction limit), as the maximum of the *n* background measurements, where γ is a function of *n, m*, and *k*. The objective of the analysis is thus how to select the combinations of *n, m,* and *k* that satisfy the conditions γ is greater than or equal to a certain confidence level (for example, 95 percent).

Following Gibbons (1990) derivation, let $V_{(\max,\, n)}$ represent the maximum value of the indicator parameter obtained out of a background sample of size *n* and $U_{(\min,\, m)}$ represent the minimum value out of a monitoring well sample of size *m*. The confidence level for the simultaneous upper prediction is given as (Gibbons, 1990)

$$\Pr\left(U_{1(\min,m)} \le V_{(\max,n)}, U_{2(\min,m)} \le V_{(\max,n)}, \ldots, U_{k(\min,m)} \le V_{(\max,n)} \right) = \gamma$$

This equation indicates that for a fixed number of background samples, one must increase *m* to achieve a desired confidence level. Gibbons (1990) mathematically gave this probability expression based on using a variant of the multivariate hypergeometric distribution, which is written as

$$\gamma = \frac{n}{km+n} \sum_{j_1=1}^{m} \sum_{j_2=1}^{m} \cdots \sum_{j_k=1}^{m} \frac{\binom{m}{j_1}\binom{m}{j_2}\cdots\binom{m}{j_k}}{\binom{km+n-1}{\sum_{i=1}^{k} j_i + n - 1}} \qquad (9)$$

where the notation $\binom{m}{j}$ denotes the number of ways in which j objects can be selected from m objects, calculated as $\frac{m!}{j!\ (m-j)!}$. Equation (9) relates the confidence level to the size of the background samples, the number of downgradient monitoring wells and the number of samples (or resamples) allowed for each monitoring well. It can be used in a number of ways, the most important of which is to guard against false positives. That is, the main advantage of this approach is that detection of a contaminant in a monitoring well does not warrant special attention or require corrective actions unless it is shown statistically using the required number of resamplings that the positive signal is indeed attributed to the contaminant source.

The main problem in Equation (9) is that as the number of monitoring wells, k, gets large, the number of terms in the probability sum gets extremely large, which restricts the use of Equation (9) to cases where the number of monitoring wells and number of required resamplings are small. However, Gibbons (1990) provided a reasonable approximation to Equation (9) that makes it computationally feasible to deal with large numbers of wells and resamplings. The approximated probability is given in Gibbons (1990) as

$$\gamma \cong \left[\frac{n}{m+n} \sum_{j=1}^{m} \frac{\binom{m}{j}}{\binom{m+n-1}{j+n-1}} \right]^{k} \qquad (10)$$

To show the use of Equations (9) and (10), Gibbons provided the following hypothetical example. Assume a facility that has two upgradient (e.g., background) wells and five downgradient (e.g., monitoring) wells. The monitoring wells are assumed to be sampled quarterly and are assumed to produce relatively independent measurements. For the upgradient wells, it is assumed that two years of quarterly monitoring have taken place, yielding 16 background measurements. Using Equation (9) under the assumptions that 1) the distribution of the indicator parameter is continuous, 2) the distribution of groundwater quality is the same in the upgradient and downgradient locations, and 3) the measurements are independent, the probability that the five new monitoring values (one at each downgradient well) will be less than the maximum of the 16 background samples is 0.762. This value indicates a high false positive rate (e.g., 1.0 – 0.762 = 0.238). However, if in this 23.8 percent of the cases in which a false positive result is obtained it is allowed that the facility owner/operator resamples the well and if the new measurement is below the maximum of the 16 background values, the facility could return to normal monitoring (Gibbons, 1990). With a single resampling, the probability that at least one of two measurements in each well will be less than the maximum of the 16 background measurements is obtained from Equation (10) as

0.968 or a false positive rate of only 3.2 percent, which is much smaller than the 23.8 percent obtained above.

This approach and one modified in Gibbons (1992) have some potential benefits if applied at Shoal. During the 5-year proof-of-concept period, existing wells that are mostly in the upgradient direction relative to the cavity can be sampled on a regular basis for naturally occurring radionuclides that are also produced by the nuclear test. This sampling will provide the background data that can be used to statistically identify a potential false positive signal. This will help determine when detection monitoring can continue and when more analysis and evaluation are required. Also, this approach can be used to design the optimal resampling plan for the site. For example, if one has seven background samples and there are four monitoring wells in the downgradient direction (e.g., long-term monitoring wells at Shoal), the number of resamples required to provide a 95 percent confidence level is only one. This means that when at least one out of two samples in each of the four monitoring wells is below the maximum of the seven background samples, there is a 95 percent confidence level that the samples that exceed this maximum are false positive signals.

4. SUMMARY AND CONCLUSIONS

The flow and transport model of Shoal is used to design a three-well monitoring network to be part of the long-term monitoring network for the site and achieve two objectives. The first objective is to detect the presence of radionuclides in case they migrate to the monitoring well locations (detection monitoring). The second objective is to provide field data to compare with model predictions as part of the model validation process. In addition, during the first five years of operation, proof-of-concept monitoring is required where measurement of field parameters will be used to demonstrate that the model is capable of making reasonable predictions that fall within an acceptable level of confidence.

Using three different quantitative approaches and the numerical groundwater flow and transport model developed for Shoal, three new monitoring well locations have been identified from 76 different networks. The selected wells are assigned names MV-1 (well 2 in the previous analysis), MV-2 (well 4), and MV-3 (well 6), designating their purpose for monitoring and validation, as compared to the HC wells. These locations may be slightly modified to avoid practical limitations encountered when selecting drill sites. In addition to the proposed new wells, existing wells HC-1 and HC-4 are proposed for inclusion in the network. Neither had good individual well performance, but they are low-cost additions that will provide additional areal coverage.

In addition to the quantitative analyses using the numerical model, the development of the monitoring network for Shoal will also be subject to qualitative hydrogeologic interpretation during implementation. Insight developed from knowledge of the hydrogeologic environment will directly affect the final well completions. For example, transport through fractures is the pathway of concern through the granite. Although the simulation and probability-based approaches indicate that the best vertical location to screen the monitoring wells spans intervals from elevations of 1,000 to 1,155 m, any large fracture zone encountered during drilling will be carefully evaluated as a potential screen location, whether or not it is at that exact vertical horizon predicted by the model. Other factors that will be considered during drilling and testing the monitoring wells are the hydraulic heads encountered and the identification of faults or other significant hydrogeologic features. As this

information will only be available during the fieldwork, it will be incorporated in the monitoring well design at the time of well installation.

Finally, it should be noted that the CADD-CAP for Shoal, including the compliance boundary, is not yet approved. Should the compliance boundary change from the 1,000-year MCL contaminant boundary, well locations may also need to change. However, the analysis reported here provides a number of alternatives with reasonable detection efficiency.

REFERENCES

Ahlfeld, D.P. and G.F. Pinder, 1988. A groundwater monitoring network design algorithm. Report 87-WR-4, Department of Civil Engineering and Operations Research, Princeton University, Princeton, NJ.

Bernstein, B.B. and J. Zalinski, 1983. An optimum sampling design power tests for environmental biologists. *Environmental Management*, 16, 35-43.

Borg, I.Y., R. Stone, H.B. Levy and L.D. Ramspott, 1976. Information Pertinent to the Migration of Radionuclides in Ground Water at the Nevada Test Site, Part 1: Review and Analysis of Existing Information. Lawrence Livermore National Laboratory, UCRL-52078 Pt. 1, 216 p.

Carroll, R., T. Mihevc, G. Pohll, B. Lyles, S. Kosinski, and R. Niswonger, 2000. Project Shoal Area Tracer Test Experiment. Desert Research Institute, Publication No. 45177, DOE/NV/ 13609--05, 35p.

Chapman, J.B., K. Pohlmann, G. Pohll, A.E. Hassan, P. Sanders, M. Sanchez and S. Jaunarajs, 2002. Remediation of the Faultless underground nuclear test: Moving forward in the face of model uncertainty. In Proceedings of the Waste Management Conference, WM'02, Tucson, Arizona.

Everett, L.G., 1980. Groundwater monitoring. General Electric Company, Schenectady, NY.

FFACO, 2000. Federal Facilities Agreement and Consent Order, Appendix VI: Corrective Action Strategy.

Gibbons, R.D., 1990. A general statistical procedure for ground-water detection monitoring at waste disposal facilities. *Ground Water*, 38(3):235-343.

Hassan, A., K. Pohlmann and J. Chapman, 2002. Modeling Groundwater Flow and Transport of Radionuclides at Amchitka Island's Underground Nuclear Tests: Milrow, Long Shot, and Cannikin. Desert Research Institute, Division of Hydrologic Sciences, Publication No. 45172, DOE/NV/11508--51.

Hassan, A.E., 2003. Long-term Monitoring Plan for the Central Nevada Test Area. Desert Research Institute, Division of Hydrologic Sciences, Publication No. 45201, DOE/NV/13609-30, 56p.

Hassan, A.E., 2004. Validation, Proof-of-Concept, and Postaudit of the Groundwater Flow and Transport Model of Project Shoal Area. Desert Research Institute, Division of Hydrologic Sciences, Publication No. 45206, DOE/NV/13609-35.

Hudak, P.F., 1994. A method for monitoring ground water quality near waste storage facilities. *Environmental Monitoring and Assessment*, 30, 197-210.

Hudak, P.F., 1996. A method for designing detection monitoring networks in layered aquifers with non-uniform flow. *J. Environ. Manag*., 48:341-355.

Hudak, P.F., 2001. Effect of groundwater velocity on sampling intervals for contaminant-detection networks in aquifers. *J. Environ. Sci. Health*, 36(1):117-122.

IT Corporation, 2000. 1999 Well Installation Report, Project Shoal Area, Churchill County, Nevada. Prepared for U.S. Department of Energy, Nevada Operations Office. Las Vegas, Nevada, ITLV/13052-097, variable paging.

Kinzelbach, W., 1988. The random walk method in pollutant transport simulation. In Groundwater Flow and Quality Modeling. E. Custodio, A. Gurgui, J.P. Lobo Ferreira, and D. Reidel (eds.), Norwell, MA, 227-246.

Knopman, D., C.I. Voss and S.P. Garabedian, 1991. Sampling design for groundwater solute transport: Tests of methods and analysis of Cape Cod tracer test data. *Water Resources Research*, 27(5), 925-949.

LaBolle, E., G. Fogg and A.F.B. Tompson, 1996. Random-walk simulation of solute transport in heterogeneous porous media: Local mass-conservation problem and implementation methods. *Water Resources Research*, 32:583-593.

LaBolle, E., J. Quastel, G. Fogg and J. Gravner, 2000. Diffusion processes in a composite porous media and their integration by random walks: Generalized stochastic differential equations with discontinuous coefficients. *Water Resources Research*, 36:651-662.

Lee, G.F. and R.A. Jones, 1983a. Guidelines for sampling groundwater. *Journal of Water Pollution Control Federation*, 55(1), 92-96.

Lee, G.F. and R.A. Jones, 1983b. Active versus passive water quality monitoring programs for wastewater discharges. *Journal of Water Pollution Control Federation*, 55(4), 405-407.

Loaiciga, H.A., R.J. Charbeneau, L.G. Everett, G.E. Fogg, B.F. Hobbs and S. Rouhani, 1992. Review of groundwater quality monitoring network design. *J. Hydraul. Eng*., 118(1), 11-37.

Mahar, P.S. and B. Datta, 1997. Optimal monitoring network and groundwater-pollution source identification. *Journal of Water Resources Planning and Management*, 123(4), 199-207.

Mar, B.W., R.R. Horner, J.S. Richey, R.N. Palmer and D.P. Lettenmaier, 1986. Data acquisition. *Environmental Science and Technology*, 20(6), 545-551.

Massmann, J. and R.A. Freeze, 1987a. Groundwater contamination from waste management sites: The interaction between risk-based engineering design and regulatory policy. 1. Methodology. *Water Resources Research*, 23(2), 351-367.

Massmann, J. and R.A. Freeze, 1987b. Groundwater contamination from waste management sites: The interaction between risk-based engineering design and regulatory policy. 2. Results. *Water Resources Research*, 23(2), 368-380.

McLaughlin, D. and W. Graham, 1986. Design of cost-effective programs for monitoring groundwater contamination. In Integrated Design of Hydrological Networks, IAHS Publication No. 158, 231-246.

Meyer, P. and E.D. Brill, Jr., 1988. A method for locating wells in a groundwater monitoring network under conditions of uncertainty. *Water Resources Research*, 24(8), 1277-1282.

Meyer, P.D., R. Ranjithan, A.J. Valocchi and J.W. Eheart, 1989. Groundwater monitoring network design using coupled Monte Carlo simulation and optimization. In Proceedings of the 1989 National Conference on Hydraulics Engineering, M.A. Ports (ed.), ASCE, New York, NY, 404-409.

Mihevc, T., G. Pohll and B. Lyles, 2000. Project Shoal Area Field Data Summary Report. Desert Research Institute, Publication No. 45175, DOE/NV/11508--54, 258p.

Olea, R.A., 1984. Sampling design optimization for spatial functions. *Mathematical Geology*, 16(4), 365-391.

Pohll, G., J. Chapman, A. Hassan, L. Papelis, R. Andricevic and C. Shirley, 1998. Evaluation of Groundwater Flow and Transport at the Shoal Underground Nuclear Test: An interim report. Desert Research Institute, Division of Hydrologic Sciences, Publication No. 45162, DOE/NV/11508-35.

Pohll, G., A.E. Hassan, J.B. Chapman, C. Papelis and R. Andricevic, 1999a. Modeling groundwater flow and radioactive transport in a fractured aquifer. *Groundwater,* 37(5): 770-784.

Pohll, G., J. Tracy and F. Forsgren, 1999b. Data Decision Analysis: Project Shoal. Desert Research Institute, Division of Hydrologic Sciences, Publication No. 45166, DOE/NV/11508--42, 27p.

Pohll, G., K. Pohlmann, J. Daniels, A. E. Hassan and J. Chapman, 2002. Contaminant and Compliance Boundaries at the Faultless Underground Nuclear Test. Desert Research Institute, Division of Hydrologic Sciences, Publication No. 45196, DOE/NV/13609--24, pp. 50.

Pohll, G. and K. Pohlmann, 2004. Contaminant Boundaries at the Shoal Underground Nuclear Test. Desert Research Institute, Letter Report, pp. 19

Pohlmann, K.F., A.E. Hassan and J.B. Chapman, 1999. Evaluation of Groundwater Flow and Transport at the Faultless Underground Nuclear Test, Central Nevada Test Area. Desert Research Institute, Division of Hydrologic Sciences, Publication No. 45165, DOE/NV/11508--41, pp. 129.

Pohlmann, K., G. Pohll, J. Chapman, A.E. Hassan, R. Carroll and C. Shirley, 2004. Modeling to Support Groundwater Contaminant Boundaries for the Shoal Underground Nuclear Test. Desert Research Institute, Division of Hydrologic Sciences, Publication No. 45184-revised, pp. 197.

Reimus, P., G. Pohll, T. Mihevc, J. Chapman, M. Haga, B. Lyles, S. Kosinski, R. Niswonger and P. Sanders, 2003. Testing and parameterizing a conceptual model for solute transport in a fractured granite using multiple tracers in a forced-gradient test. *Water Resources Research*, 39(12):1356-1370.

Todd, D.K., R.M. Timlin, K.D. Schmidt and L.G. Everett, 1976. Monitoring groundwater quality: Monitoring methodology. U.S. Environmental Protection Agency, Las Vegas, Nevada.

Tompson, A.F.B. and L.W. Gelhar, 1990. Numerical simulation of solute transport in three dimensional randomly heterogeneous porous media. *Water Resources Research*, 26(10):2541-2562.

U.S. Department of Energy (DOE), 1998a. Data Report Project Shoal Area Churchill County, Nevada. Nevada Operations Office, Environmental Restoration Division, DOE/NV--505, variable paging.

U.S. Department of Energy (DOE), 1998b. Corrective Action Investigation Plan for Corrective Action Unit 447: Project Shoal Area, Nevada Subsurface Site. Nevada Operations Office, Environmental Restoration Division, DOE/NV--513, 71p.

U.S. Department of Energy (DOE), 1999. Addendum to the Corrective Action Investigation Plan for Corrective Action Unit 447: Project Shoal Area, Nevada Subsurface Site. Nevada Operations Office, Environmental Restoration Division, DOE/NV--513-ADD, 10p.

U.S. Department of Energy (DOE), 2000. United States Nuclear Tests, July 1945 through September 1992. DOE/NV-209, rev. 15, Nevada Operations Office.

U.S. Environmental Protection Agency (EPA), 1986. RCRA Groundwater Monitoring Technical Enforcement Guidance Document. Office of Solid Water Emergency Response, U.S. Environmental Protection Agency, Washington, D.C.

U.S. Environmental Protection Agency (EPA), 1994. RCRA Groundwater Monitoring. Government Institutes, Rockville, MD.

van Dernoot and C. Williams, 1988. Drowning in groundwater environmental monitoring costs? *Water Eng. Manag*, May, 44-45.

Ward, R.C., J.C. Loftis and G.B. McBride, 1986. The data-rich but information-poor syndrome in water quality monitoring. *Environmental Management*, 10(3), 291-297.

Wilson, C.R., C.M. Einberger, R.L. Jackson and R.B. Mercer, 1992. Design of groundwater monitoring networks using the Monitoring Efficiency Model (MEMO). *Ground Water*, 30:965-970.